RESEARCH ARTICLE

Key Points:
- Wintertime organic aerosol (OA) was almost as oxidized as in summer studies, with wood burning OA being an important contributor to primary OA
- SOA formation rate and amount is similar to summer (accounting for lower OH). A box model reproduces SOA, but fast chemistry may be missing
- The default GEOS-Chem formulation with nonvolatile POA shows large errors. The SIMPLE and semivolatile parameterizations perform better

Supporting Information:
- Supporting Information S1

Correspondence to:
J. L. Jimenez,
jose.jimenez@colorado.edu

Sources and Secondary Production of Organic Aerosols in the Northeastern United States during WINTER

J. C. Schroder[1,2], P. Campuzano-Jost[1,2], D. A. Day[1,2], V. Shah[3], K. Larson[3], J. M. Sommers[4,5], A. P. Sullivan[6], T. Campos[7], J. M. Reeves[7], A. Hills[7], R. S. Hornbrook[7], N. J. Blake[8], E. Scheuer[9], H. Guo[10], D. L. Fibiger[1], E. E. McDuffie[1,2,11], P. L. Hayes[4], R. J. Weber[10], J. E. Dibb[9], E. C. Apel[7], L. Jaeglé[3], S. S. Brown[2,11], J. A. Thornton[3], and J. L. Jimenez[1,2]

[1]Cooperative Institute for Research in Environmental Sciences, University of Colorado Boulder, Boulder, CO, USA, [2]Department of Chemistry, University of Colorado Boulder, Boulder, CO, USA, [3]Department of Atmospheric Sciences, University of Washington, Seattle, WA, USA, [4]Department of Chemistry, Université de Montréal, Montréal, Quebec, Canada, [5]Air Quality Research Division, Environment and Climate Change Canada, Toronto, Ontario, Canada, [6]Department of Atmospheric Science, Colorado State University, Fort Collins, CO, USA, [7]Atmospheric Chemistry Observation and Modeling Laboratory, National Center for Atmospheric Research, Boulder, CO, USA, [8]Department of Chemistry, University of California, Irvine, CA, USA, [9]Institute for the Study of Earth, Ocean, and Space, University of New Hampshire, Durham, NH, USA, [10]School of Earth and Atmospheric Sciences, Georgia Institute of Technology, Atlanta, GA, USA, [11]Chemical Science Division, NOAA Earth System Research Laboratory, Boulder, CO, USA

Abstract Most intensive field studies investigating aerosols have been conducted in summer, and thus, wintertime aerosol sources and chemistry are comparatively poorly understood. An aerosol mass spectrometer was flown on the National Science Foundation/National Center for Atmospheric Research C-130 during the Wintertime INvestigation of Transport, Emissions, and Reactivity (WINTER) 2015 campaign in the northeast United States. The fraction of boundary layer submicron aerosol that was organic aerosol (OA) was about a factor of 2 smaller than during a 2011 summertime study in a similar region. However, the OA measured in WINTER was almost as oxidized as OA measured in several other studies in warmer months of the year. Fifty-eight percent of the OA was oxygenated (secondary), and 42% was primary (POA). Biomass burning OA (likely from residential heating) was ubiquitous and accounted for 33% of the OA mass. Using nonvolatile POA, one of two default secondary OA (SOA) formulations in GEOS-Chem (v10-01) shows very large underpredictions of SOA and O/C (5×) and overprediction of POA (2×). We strongly recommend against using that formulation in future studies. Semivolatile POA, an alternative default in GEOS-Chem, or a simplified parameterization (SIMPLE) were closer to the observations, although still with substantial differences. A case study of urban outflow from metropolitan New York City showed a consistent amount and normalized rate of added OA mass (due to SOA formation) compared to summer studies, although proceeding more slowly due to lower OH concentrations. A box model and SIMPLE perform similarly for WINTER as for Los Angeles, with an underprediction at ages <6 hr, suggesting that fast chemistry might be missing from the models.

1. Introduction

Atmospheric aerosols are known to affect human health (Pope III et al., 2002), visibility (Boers et al., 2015), and climate (Myhre et al., 2013). In particular, considerable uncertainty remains in the radiative forcing by aerosols. Therefore, efforts to improve our understanding of aerosol sources, transport, processing, and forcing continue to be important.

Field studies provide our primary source of information on aerosol concentrations, sources, and evolution in the real atmosphere. However, the large majority of intensive field studies at northern midlatitudes have been conducted in warmer and more photochemically active times of the year, especially those targeting detailed organic aerosol (OA) composition, sources, and evolution. Several studies that have looked at seasonal variations of aerosol composition around the world have shown distinct differences between summer and winter (Allan, Alfarra, et al., 2003; Hu et al., 2016; Huang et al., 2013; Poulain et al., 2011; Takegawa et al., 2005; Weimer et al., 2006). Midlatitude winter has significantly lower temperatures, reduced solar radiation, and often more precipitation, all of which can significantly alter the processes that govern the production, processing, and lifetimes of aerosols. In addition, dry deposition velocities of semivolatile species have been shown to be significantly different for some species in winter (Jaeglé et al., 2017). Although in the last

few decades there have been a number of wintertime studies of aerosols in Asia (e.g., Cao et al., 2003; Kim et al., 2017; Rengarajan et al., 2007, 2011; Takegawa et al., 2005; Xu et al., 2016; Zhang et al., 2015) and Europe (e.g., Allan, Alfarra, et al., 2003; Bardouki et al., 2003; Castro et al., 1999; Crippa et al., 2013; Lanz et al., 2008; Louvaris et al., 2017; Viana et al., 2006), very few have been conducted in North America (e.g., Budisulistiorini et al., 2016; Öztürk et al., 2013; Song et al., 2001; Strader et al., 1999; Tan et al., 2002; Weimer et al., 2006; Xu et al., 2015). However, most of the North American studies were conducted at least a decade ago, and none were conducted in the northeastern United States (NE-US). Moreover, of these wintertime aerosol studies, only a few have investigated the source contributions of OA and none have investigated the rates of secondary OA (SOA) formation from wintertime pollution emissions. In general, wintertime studies have shown lower total concentrations of submicron aerosols than summer. Similar to summer studies, OA is a major (and often the largest) fraction of submicron aerosol in the winter, typically with increases in primary OA (POA), mostly driven by increases in biomass burning OA (BBOA) from residential wood burning (Bressi et al., 2016; Budisulistiorini et al., 2016; Crippa et al., 2013; Lanz et al., 2008; Xu et al., 2015, 2016). The amount of oxidized OA (OOA) observed in warmer months of the year has been documented extensively in the literature, throughout much of the world (Jimenez et al., 2009, and references within). The amount of OOA reported in urban environments varies greatly depending on the geographical location, but in general, accounts for approximately 50–80% of the total OA mass during the summer. In the winter, fewer studies have reported on measurements of urban OOA (Crippa et al., 2013; Kim et al., 2017; Öztürk et al., 2013; Pirjola et al., 2017; Zhang et al., 2015), showing fractions of OA mass between 20% and 70%.

OOA is often used as a proxy for SOA, which forms from gas-to-particle conversion via gas-phase or aqueous-phase mechanisms. During the summer, the solar radiation, temperature, and vegetation leaf coverage are highest, resulting in biogenic emissions that contribute significantly to local and regional chemistry (Ding et al., 2016; Ehn et al., 2014; Henze et al., 2008; Marais et al., 2016; Palm et al., 2016), even in polluted regions. In winter, however, biogenic emissions are often much smaller or negligible (Ding et al., 2016, 2017; Guenther et al., 2012) due to reduced sunlight, temperatures, and foliage. Several studies have investigated the production of urban SOA in polluted areas under warm weather (Cevik et al., 2016; DeCarlo et al., 2010; Freney et al., 2014; Hayes et al., 2013, 2015; Kleinman et al., 2008; Ma et al., 2017; McMeeking et al., 2012; Weber et al., 2007). However, no study (to the best of our knowledge) has presented a detailed evaluation on the regional production of SOA during winter using aircraft data.

Chemical transport models often underpredict OA concentrations (Tsigaridis et al., 2014), particularly near and downwind of anthropogenic sources. Recently, significant efforts have gone into improving the capability of global models to better predict OA evolution by implementing a variety of SOA formation and aging schemes, with differing levels of complexity (Hodzic et al., 2016; Hodzic & Jimenez, 2011; Jo et al., 2013; Kim et al., 2015; Pye & Seinfeld, 2010; Tsigaridis et al., 2014; Tsimpidi et al., 2016). As part of the AeroCom II model intercomparison, Tsigaridis et al. (2014) compared OA from 31 different global chemical transport and general circulation models. That study found that in general, global models can reasonably predict the dominantly secondary nature of OA, yet the absolute amount of OA is still significantly underpredicted, with a mean normalized bias of −0.62 for all surface urban data compared, −0.15 in remote regions, and −0.30 in marine locations. Although the spatial resolution of most 3-D models is too coarse to accurately capture OA mass concentrations in smaller urban areas, megacities like Los Angeles, Beijing, or New York City are of more similar size to model resolutions thus reducing error in the comparisons. In addition, when examining seasonality, the models are unable to predict observed wintertime trends in several urban locations, leading the authors to hypothesize that capturing the relative importance of SOA versus anthropogenic POA is a critical factor for the models to more accurately simulate seasonal trends. Similarly, Tsimpidi et al. (2016) used the general circulation model ECHAM combined with the Modular Earth Submodel System (MESSy) MESSy to evaluate modeled OA combustion sources compared to 84 different observational data sets. From that study, the authors concluded that a major weakness in the model is the poor ability to simulate wintertime POA and SOA concentrations, which they hypothesized is due to the model missing an important wintertime OA source or SOA formation pathway.

Wintertime measurements are needed to better understand the changes in aerosol sources, atmospheric processing, and lifetimes, and to better constrain regional and global models to more accurately predict wintertime concentrations and seasonal differences. Here we present wintertime submicron aerosol composition measurements from the NE-US from an airborne platform. We compare wintertime concentrations to

previously reported summertime studies, apply source apportionment analysis to explore the sources of OA and contrast them to observations from warmer periods of the year, investigate the evolution of OA (amount and composition), and compare it to predictions from the GEOS-Chem model. We report the first aircraft measurements of SOA production efficiency in winter from a case study of urban outflow from New York City, and we compare it to a box model and a simple parameterization of SOA formation.

2. Methods

The Wintertime INvestigation of Transport, Emissions, and Reactivity (WINTER) aircraft campaign (WINTER, 2018) took place out of the NASA Langley Research Center (Hampton, VA) from 1 February to 15 March 2015 aboard the National Center for Atmospheric Research (NCAR) C-130 aircraft. Aircraft studies provide insight into changes in chemical properties and processes spatially, both vertically and horizontally, that stationary ground campaigns cannot. The campaign objectives for WINTER were to characterize both gas-phase and particle-phase wintertime emissions and chemical transformations. Thirteen research flights (RF) were carried out (see supporting information Figure S1), with 102 hr of sampling time. Aircraft parameters and ambient meteorological measurements were provided by the NCAR Research Aviation Facility. More details about WINTER, the payload, and logistics can be found online, and all data are public and available at (WINTER-Data, 2018). Data reported here are at standard temperature (273 K) and pressure (1,013 mbar) (STP), and all linear fits within this manuscript use the orthogonal distance regression method.

In general the 2015 winter season over the NE-US was colder than average. The NCEP/NCAR reanalysis data indicate that surface temperatures in the NE-US for February 2015 were about 5 °C colder than the February 1981–2010 average.

2.1. Instrumentation
2.1.1. PM_1 Nonrefractory Composition (AMS)

A highly customized high-resolution time-of-flight aerosol mass spectrometer (Aerodyne Research Inc., hereafter referred to as "AMS") measured nonrefractory composition of PM_1 (NR-PM_1; DeCarlo et al., 2006; Dunlea et al., 2009). The theory and operation of the AMS, including the key adaptations for aircraft sampling, have previously been described in detail (Canagaratna et al., 2007; DeCarlo et al., 2006; Dunlea et al., 2009; Jayne et al., 2000; Kimmel et al., 2011) and is only briefly summarized here. Ambient particles were sampled through an NCAR High-Performance Instrumented Airborne Platform for Environmental Research Modular Inlet (HIMIL, 2018; Moharreri et al., 2014) at a flow rate of 10 L/min, into a pressure-controlled inlet operated at 325 Torr (Bahreini et al., 2008). The particles were then focused into the high-vacuum region of the mass spectrometer through an aerodynamic lens and transmitted into a detection chamber, where particles impacted on a porous tungsten standard vaporizer (600 °C). Nonrefractory species in the particles were flash vaporized and then ionized with 70-eV electron impact ionization. The generated ions were then extracted and analyzed by time-of-flight mass spectrometry. The air residence time from the outside tip of the HIMIL inlet to the vaporizer was 0.5–0.6 s, depending on altitude. Transmission of particles through the AMS inlet and lens was similar to previous publications for well-performing instruments (Figure S2; Hu et al., 2017).

During WINTER, the AMS was operated in the Fast Mass Spectrum mode (Kimmel et al., 2011) in order to obtain high time resolution measurements (1 Hz). For more information on Fast Mass Spectrum operation see supporting information section S1.1 and Figure S3. For all flights the AMS sampled in V mode with a resolution of 2,300 at m/z 44 and 2,900 at m/z 184. Collection efficiency (CE) was estimated with the algorithm of Middlebrook et al. (2012; supporting information section S1.1.2). Relative ionization efficiencies (Canagaratna et al., 2007) for sulfate, ammonium, and chloride were determined from repeated infield calibrations (Figure S5). Typical detection limits during WINTER were 137 (57) ng/sm^3 for sulfate (SO4), 12 (5) ng/sm^3 for ammonium (NH4), 69 (30) ng/sm^3 for nitrate (NO3), 77 (32) ng/sm^3 for chloride (Chl), and 474 (194) ng/sm^3 for OA for a 1-s (1-min) sampling interval (sm^3 refers to cubic meters at standard temperature and pressure). Note that the charge symbols are not used (i.e., we write NO3 and not NO_3^-), as there can be contributions from organonitrates and organosulfates to AMS NO3 and SO4, respectively (e.g., Docherty et al., 2011; Fry et al., 2013; Liao et al., 2015). Accuracy for aircraft AMS measurements of inorganic (organic) species is estimated at ±35% (±38%; Bahreini et al., 2009). Semirefractory species, such as NaNO3 (sodium nitrate) and Na2SO4 (sodium sulfate), are inefficiently detected by the AMS (Hayes et al., 2013). AMS data have sometimes been used to estimate the fractions of ammonium nitrate and

organic nitrates using the measured NO_2^+/NO^+ ion ratio (Farmer et al., 2010; Fry et al., 2013). However, in this study, the presence of particulate nitrite (Guo et al., 2016) and the likely partial detection of $NaNO_3$ made that method indeterminate. For that reason, in addition to total measured nitrate, estimates were made of total inorganic nitrate concentrations based on comparisons of the AMS data to the ion chromatography-based instruments. For a complete discussion on the measured nitrate during WINTER see supporting information section S1.1.4.2 and Figures S8–S10. Several corrections were made to the AMS data to account for recently discovered, small vaporizer artifacts that affect OA and chloride quantification, also discussed in supporting information section S1.1.3 and Figure S6. The AMS was fully operational for all flights during WINTER except RF05 leading to an overall 96% data coverage.

2.1.2. Collocated WINTER Measurements Used in This Study

PM_1 size-resolved volume concentration was measured by two optical particle counters mounted on the wings of the C-130, an Ultra High Sensitivity Aerosol Spectrometer (Droplet Measurement Technology; Brock et al., 2016; Cai et al., 2008) and a Passive Cavity Aerosol Spectrometer Probe (PCASP-100X, Droplet Measurement Technologies; Liu et al., 1992). The Ultra High Sensitivity Aerosol Spectrometer, as used in this study, had a geometric size range of 0.075–1 μm and the PCASP measured from 0.1–3 μm (geometric). Only data collected within bins that correspond to a vacuum aerodynamic diameter of ≤1 μm were used in our analyses, and both particle counters were corrected for differences in inlet transmission to achieve more accurate comparisons with the AMS (Hu et al., 2017; Knote et al., 2011; see supporting information S1.1.4.1 for more details). Both probes substantially dry particles on the way to the laser, due to their diffusing intakes up front (which slow the air, leading to heating), sample flow passage though warm anti-iced components, internal components near room temperature, and recirculating sheath flow at that internal temperature. Thus, the aerosol volume measured by these probes approximately corresponds to the dry particle volume and does not include liquid water that was present on those particles under ambient conditions (Strapp et al., 1992). Both instruments were serviced and calibrated using polystyrene latex spheres (refractive index [n] = 1.595) by the manufacturer just prior to deployment. To more accurately estimate the total volume concentrations of ambient particles, both instruments were size corrected (1.12×diameter) similar to Kupc et al. (2017) and Liu et al. (2017) to estimate the measured diameters with a more atmospherically relevant refractive index (dry ammonium sulfate, n = 1.53 [Hand & Kreidenweis, 2002]).

PM_1 water-soluble mass concentration was measured by two particle-into-liquid samplers (PILS). The first PILS-IC, described in Guo et al. (2016), was coupled to an online ion chromatograph ("Online-PILS-IC," Metrohm 761 Compact ICs; Hennigan et al., 2006; Orsini et al., 2003; Peltier et al., 2007) and reported the concentrations of sulfate, nitrate, and chloride at a time resolution of 3 min. The second PILS-IC was coupled to a Bretchel fraction collector system (Sorooshian et al., 2006) for offline analysis ("Offline-PILS-IC") of levoglucosan and the inorganic ions sodium, ammonium, potassium, chloride, nitrate, and nitrite at a time resolution of 2 min (Sullivan et al., 2017). The inorganic ions were measured by anion/cation-exchange chromatography (Guo et al., 2016) and levoglucosan by high-performance anion-exchange chromatography-pulsed amperometric detection (Sullivan, Frank, Kenski, et al., 2011; Sullivan, Frank, Onstad, et al., 2011; Sullivan et al., 2014). PM_5 bulk aerosol composition was measured offline from filter samples ("SAGA Filters"; Dibb, 2003; Dibb et al., 2002), at a time resolution of ~7 min. Volatile organic compounds (VOCs) were measured for 35 s every 2 min with the Trace Organic Gas Analyzer (Apel et al., 2010). For more details on specific WINTER configurations for SAGA-Filters and Trace Organic Gas Analyzer see supporting information sections S1.2 and S1.3, respectively. Carbon monoxide (CO) was quantified by vacuum ultraviolet resonance fluorescence with a customized commercial instrument (Aero-Laser AL-5002), at a rate of 0.5 Hz. NO, NO_2, and NO_y were measured by a six-channel cavity ring-down instrument. NO_2 was measured directly by laser absorption at 405 nm. NO was converted and measured as NO_2 after an addition of excess O_3 (Wagner et al., 2011). NO_y was thermally dissociated in a heated quartz inlet (650 °C) and similarly converted and measured as NO_2 with an addition of excess O_3 (Wild et al., 2014; Womack et al., 2017).

2.2. Modeling

2.2.1. FLEXPART

European Reanalysis-Interim meteorological fields with a horizontal resolution of 0.5° × 0.5°, a temporal resolution of 3 hr, and 60 vertical hybrid pressure-terrain following coordinate levels were used to drive

the FLEXPART Lagrangian particle dispersion model (Seibert & Frank, 2004; Stohl et al., 1998, 2005; Stohl & Thomson, 1999). The FLEXPART output has a resolution of 0.1° × 0.1° over the domain of 100.0°W to 60.0°W and 25.0°N to 50.0°N and includes residence time in the surface layer (<100, <250, and <500 m). Thirty thousand back trajectory particles were released every 20 s, or for every altitude change of 100 m, along the aircraft flight tracks. The back trajectories were calculated for 48 hr with outputs at 15-min intervals.

2.2.2. GEOS-Chem

GEOS-Chem is a 3-D chemical transport model driven by assimilated meteorological fields from NASA Global Modeling and Assimilation Office (GMAO) GEOS-5 FP system (Rienecker et al., 2008). GEOS-Chem simulates the tropospheric chemistry of CO, HO_x, NO_x, VOC, O_3, BrO_x, SO_2, and aerosols (Bey et al., 2001; Park, 2003; Park et al., 2004; Parrella et al., 2012). We use GEOS-Chem v10-01 for this study. The model is run in a nested-grid configuration with a resolution of 0.5° latitude × 0.625° longitude over North America (10°N to 60°N, 130°W to 60°W), and a 4° latitude × 5° longitude resolution for the rest of the globe. Anthropogenic emissions over the United States are from U.S. Environmental Protection Agency's (EPA) 2011 Version 6 Emissions Modeling Platform based on the National Emissions Inventory (NEI) 2011 v1 (NEI, 2018) and from the Emissions Database for Global Atmospheric Research (EDGAR) v4.2 (EDGAR, 2018) for the rest of the globe.

We perform three simulations using different approaches for the simulation of OA. The first approach follows the OA simulation of Pye and Seinfeld (2010). This approach assumes nonvolatile POA and is referred to as the "Complex SOA scheme without semivolatile POA" in the GEOS-Chem online manual (GEOS-Chem, 2017) but referred to as "nvPOA" here. This approach includes SOA formation from oxidation of aromatics (benzene, toluene, and xylene), monoterpenes, sesquiterpenes, and isoprene. Aerosol yields are parameterized using a volatility basis set with saturation concentrations (C^*) at 298 K of 0.1, 1, 10, and 100 μg/m^3 and using an enthalpy of vaporization (ΔH_{vap}) of 42 kJ/mol to determine the temperature-dependent C^*. SOA formation from semivolatile volatility organic carbon (SVOC) and intermediate volatility organic carbon (IVOC), as well as heterogeneous oxidation of POA are not included in the nvPOA GEOS-Chem simulation. The second approach is similar to nvPOA with the exception of replacing nonvolatile POA with semivolatile POA, which includes partitioning of SVOC precursors to the gas phase, as well as the addition of primary IVOC (P-IVOC) precursors, with oxidation of both types of precursors to form SOA (Pye et al., 2010; Pye & Seinfeld, 2010). This approach is referred to as the "Complex SOA scheme with semivolatile POA" in the GEOS-Chem online manual (GEOS-Chem, 2017) but referred to as "svPOA" here. We assume that all SVOC emissions are captured by the NEI-2011 emissions. P-IVOC emissions are estimated by scaling naphthalene emissions, which are based on benzene emissions following Pye and Seinfeld (2010). Thus, our assumptions of IVOC emissions and chemistry are the same as those in (Pye & Seinfeld, 2010). Both Pye simulations are currently the default formulations implemented in GEOS-Chem v10-01 and can be selected by the user.

The third approach implements the SIMPLE ("SIMPLifiEd parameterization of combustion SOA") parameterization of Hodzic and Jimenez (2011) and Hayes et al. (2015) for anthropogenic and biomass burning SOA, as described by Kim et al. (2015). This approach is referred to as the "Simple SOA Scheme" in the GEOS-Chem online manual (GEOS-Chem, 2017) and is also referred to as "SIMPLE" here. This approach is planned to be the default formulation starting with v11-02 of GEOS-Chem. A single lumped SOA precursor VOC, which represents the SOA formation potential from all anthropogenic VOCs, P-IVOCs, and primary SVOCs (P-SVOCs), is emitted proportionally to anthropogenic CO, with a ratio of 0.069 g VOC (g CO)$^{-1}$. Residential burning emissions are calculated separately based on the literature, and the ratio of the precursor VOC to CO is 0.013 g VOC (g CO)$^{-1}$. The lumped VOC makes nonvolatile SOA upon OH oxidation with a 100% mass yield. Multigenerational aging is not treated explicitly in SIMPLE but is included implicitly since the parameterization is based on fits to ambient observations. The precursor VOCs are oxidized by OH with a rate coefficient of 1.25×10^{-11} cm^3 per molecule per second to form SOA, which is assumed to be nonvolatile. No SOA is formed from heterogeneous oxidation of POA. The limited net SOA formation (with OA increasing only slightly above the initial POA emissions) from biomass burning emissions implemented in SIMPLE is consistent with the overwhelming evidence from field studies of this source, including 17 aircraft studies (Cubison et al., 2011; Jolleys et al., 2012; Liu et al., 2016; Shrivastava et al., 2017). In SIMPLE, POA is modeled similarly as is in the nvPOA scenarios, and biogenic SOA is assumed to form with yields of 3% and 5% from isoprene and monoterpene oxidation, respectively, at the point of emissions.

In GEOS-Chem, OA species are represented on the basis of OC mass, and the OA mass is calculated from specified OA/OC values listed in supporting information Table S7. For comparison with the aircraft-based observations, GEOS-Chem is sampled along the flight track at 1-min intervals.

2.2.3. SOA Formation Box Model

SOA formation and evolution was also simulated with a 0-D box model, in which the oxidation of SOA precursors follows the ROB + ZHAO + MA parameterization (Ma et al., 2017). This parameterization performed reasonably well to simulate SOA formation in the Los Angeles area during CalNex-2010, with some underestimation at short photochemical ages, and agreement within the uncertainties for ages >1 day (Ma et al., 2017). The parameterization is described previously in Ma et al. (2017) and Hayes et al. (2015) and is documented in more detail in supporting information section S1.4. Briefly, oxidation products from VOCs and P-IVOCs are described by a volatility basis set where the precursor species are oxidized into five volatility bins ($C^* = 0.1, 1, 10, 100, 1,000$) according to experimental chamber measurements of OA yields for speciated VOCs and P-IVOCs (Ma et al., 2017; Presto et al., 2010). The VOC oxidation yields are corrected for vapor wall losses in the experimental chambers as described in Ma et al. (2017). Oxidation and multigeneration aging of S/IVOCs follow a bin-hopping approach where oxidation with hydroxyl radicals lowers species volatility by 1 order of magnitude for each generation (Robinson et al., 2007). Semivolatile gases are treated by equilibrium partitioning to the particle phase, using the reformulation of Pankow theory as described by Donahue et al. (2006). Initial concentrations are specified based on available WINTER measurements whenever possible or using scaled ratios to CO determined for Los Angeles when WINTER measurements are not available (see supporting information section S1.4). The SIMPLE parameterization of urban SOA formation, with the parameters of Hayes et al. (2015) derived for Los Angeles during CalNex-2010 (also used in Kim et al., 2015), is also compared to the results of the box model to evaluate the utility of the derived summertime parameters for use in wintertime conditions. We note that biogenic precursors made a very small contribution to SOA formation from urban precursors (which is what SIMPLE is parameterizing) in the CalNex study, independently of some biogenic background SOA being present over larger regional scales (Hayes et al., 2015). Biomass burning OA in field studies is observed to oxidize but without significant net gain of mass (Cubison et al., 2011; Jolleys et al., 2012; Liu et al., 2016; Shrivastava et al., 2017), and for this reason it is treated as inert in the box model.

3. Results and Discussion

3.1. Total Submicron Nonrefractory Aerosol Composition During WINTER

The average fractional composition of the nonrefractory submicron aerosol during WINTER ($\leq$0.5 km), is shown in Figure 1, along with paired summer/winter studies at several urban and rural sites around the world. The WINTER boundary layer height (BLH) was estimated to be 0.5 km (supporting information section S2.2.2 and Figure S16). The average NR-PM$_1$ ($NH_4 + NO_3 + SO_4 + Chl + OA$) concentration during WINTER in the BL was 5 μg/sm^3 with 13% NH_4, 22% NO_3, 26% SO_4, 1% Chl, and 37% OA. In contrast, the total concentration calculated from data measured in a similar region during the summer of 2011, which offers the most direct comparison with the WINTER data set, was 2.5 times greater. Four of six comparison data sets also show higher concentrations in summer than winter. On average across all data sets, winter concentrations are about 20% (by mass) lower in winter than summer, consistent with Hand et al. (2012). However, since wintertime BLH are significantly lower than summer, these results suggest that the total BL column amounts are substantially lower in winter. Other notable trends that are apparent from Figure 1 are (1) the fraction of nitrate tends to be larger (2× on average) in winter than summer. (2) Sulfate fraction is typically lower (0.7×) in winter. (3) The fraction of OA also tends to be lower (0.8×) during winter, presumably due to the importance of biogenic SOA sources in summer and faster SOA formation from anthropogenic emissions.

To investigate the components of OA present during WINTER, positive matrix factorization (PMF) analysis was performed (Ulbrich et al., 2009; Zhang et al., 2011), and four components were identified: hydrocarbon-like OA (HOA); BBOA; less-oxidized, oxidized OA (LO-OOA); and more-oxidized, oxidized OA (MO-OOA). For a discussion on the details of the PMF analysis, see supporting information section S2.1 and Figure S12. The average fraction of each OA component is shown in Figure 2a: 9% is apportioned to HOA, 33% to BBOA, 22% to LO-OOA, and 36% to MO-OOA. These data yield a total POA of 43% and 57% of the OA mass as OOA. BBOA is approximately 79% of the POA mass, which is not surprising, since residential wood burning as a source of household heating is ubiquitous in this region during
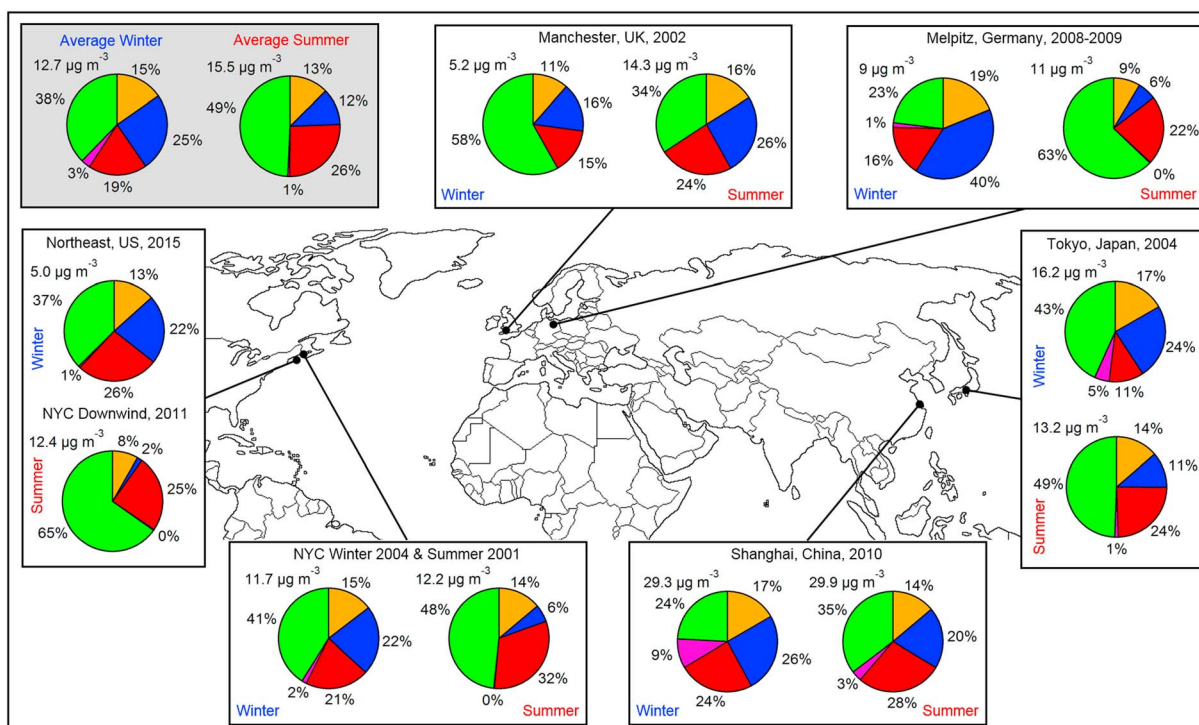
Figure 1. Overview of main NR-PM$_1$ species fractions and concentrations near the surface during WINTER ($\leq$BLH, 0.5 km) and during ground-based studies at several other Northern Hemisphere locations. Averages during WINTER are summarized under "Northeast, US, 2015, Winter." Fractional compositions are also measured with an AMS, from several urban sites: New York City (NYC; Drewnick et al., 2004; Weimer et al., 2006), Manchester, UK (Allan, Alfarra, et al., 2003; Allan, Jimenez, et al., 2003), Shanghai, China (Huang et al., 2013), and Tokyo, Japan (Takegawa et al., 2005); from an urban downwind site 80 km east of NYC (Zhou et al., 2016); and one rural/remote site in Melpitz, Germany (Poulain et al., 2011), are also shown. The averages of all sites are shown in the gray-shaded box. These sites were chosen because data from both summer and winter were available. All data used in Figure 1, with the exception of data from this study, and data for NYC Downwind US, 2011 (Zhou et al., 2016), were taken from the summary Table S1 compiled by Zhang et al. (2007; and references within).
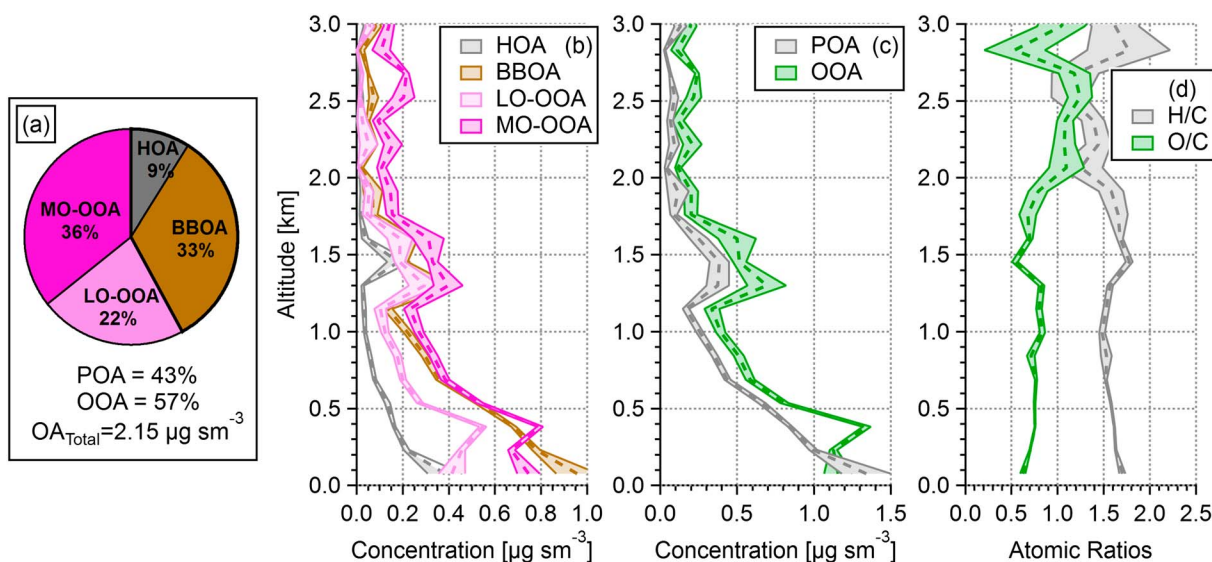

Figure 2. (a) Average fractional contribution of the identified positive matrix factorization factors to the average OA mass measured during WINTER. The thick outline surrounding HOA and BBOA represents the total fraction of primary organic aerosol (POA), while the remaining segment represents the total fraction of oxidized OA (OOA). Binned vertical concentration profiles (0–3 km) of (b) all four positive matrix factorization factors, (c) POA and OOA, and (d) atomic ratios H/C and O/C, during the WINTER campaign are also shown. The dashed lines in b–d are averages for each 153-m (500-ft) bin, and the shaded regions represent the standard error. BBOA = biomass burning OA; HOA = hydrocarbon-like OA; LO-OOA = less-oxidized, oxidized OA; MO-OOA = more-oxidized, oxidized OA.

the winter (Bond et al., 2007; Zhang et al., 2010). The contribution of BBOA to total OA is within the range (~20–40%) reported in several other studies that have reported BBOA during the winter in the United States, Asia, and Europe (Gilardoni et al., 2016; Lanz et al., 2008; Louvaris et al., 2017; Pirjola et al., 2017; Zhang et al., 2015). Some BBOA may age into OOA over regional timescales (Cubison et al., 2011). In 2015 the U.S. EPA implemented a new national policy (EPA, 2015) that increased the regulations and standards for new residential wood heating appliances, which may over time lead to a decrease of the impact of wood burning BBOA in the United States during winter. This recent change in emission standards highlights the need for continuing wintertime studies in this region to track the impact of this regulation. The fraction of OOA is similar to that observed in other winter studies, such as in urban sites in China (Zhang et al., 2015), Finland (Pirjola et al., 2017), and Switzerland (Lanz et al., 2008).

3.1.1. Spatial Patterns of Submicron Aerosol During WINTER

Figure 3 shows the spatial distributions of the submicron aerosol mass of NH_4, SO_4, NO_3, Chl, OA, and O/C measured during WINTER. In general, sulfate (Figure 3b) tends to have higher concentrations (>2 $\mu g/sm^3$) off the coast of the northeastern seaboard with intermediate concentrations ($0.75 < SO_4 < 2$ $\mu g/sm^3$) in the Ohio River Valley region, where SO_2 sources are expected to be larger. This observation is consistent with slower conversion of SO_2 to SO, due to longer lifetime of SO_2 in winter (Lee et al., 2011), which reduces the concentration of SO_4 over the source regions and increases it downwind. The distribution of nitrate (Figure 3c) shows similar regions of higher concentrations (>1.5 $\mu g/sm^3$) as sulfate, yet perhaps with higher frequency near urban regions, consistent with shorter lifetimes of NO_x in winter (Fibiger et al., 2018). Chloride (Figure 3e) was typically very low (<0.03 $\mu g/sm^3$) throughout the entire sampling region, with the exception of one flight (RF03), which was off the coast of the New York City Metropolitan Area ("NYC" hereinafter; >0.1 $\mu g/sm^3$). OA (Figure 3d) was fairly widespread during WINTER with concentrations along the eastern seaboard ranging from about 1 to 4 $\mu g/sm^3$ and elevated regions downwind of Atlanta and also in the Ohio River Valley. The extent of oxidation (O/C) of the OA was relatively consistent at around 0.8 (Figure 3f), which is surprisingly high for wintertime conditions due to expected reduced oxidant levels and photochemical activity.

Figure S13 shows the spatial distribution of the fraction of each species in NR-PM$_1$. Sulfate tends to dominate ($\geq 50\%$ of aerosol mass) in coal-fired power plant-rich regions (when over land) or when sampling far off the eastern seaboard, where the total submicron concentrations are low (<1 $\mu g/sm^3$). Nitrate is consistently above 25% when sampling in, or downwind, of major urban centers (Atlanta, Cincinnati, and Pittsburgh) and reaches $>50\%$ in the NYC Metro area. OA was ubiquitous, with fractions persistently above 25–30% and sometimes $>50\%$ when near urban centers (Atlanta and NYC). Higher fractions of OA are also often seen during high-altitude (>3 km) transits. Chloride, on the other hand, was typically $<1\%$ of the total mass throughout the entire sampling region, with the exception of one flight (RF03), which was off the coast of NYC, and reached a maximum of about 2–3%.

The vertical distributions of submicron aerosols are presented in supporting information section 2.2.1 and Figure S14a for the entire campaign, where all species show a trend of decreasing concentration with altitude. Vertical profiles were also investigated for data filtered for day, night, over land, and over the ocean sampling (Figures S14b–S14g). However, no major differences were observed for these sampling conditions.

3.1.2. Spatial Patterns of OA Composition During WINTER

To investigate the vertical distribution of OA components and the extent of oxidation of OA in the vertical, the identified PMF factors (supporting information section s2.1) as well as H/C and O/C ratios are plotted as a function of altitude in Figure 2. The OA components tend to rapidly decrease in magnitude with an increase in altitude, until an enhanced layer is observed at around 1.1 to 1.8 km. These layers are predominantly driven by a few short segments, during only a couple of flights (RF03 and RF06), and therefore, do not represent a ubiquitous campaign-wide stratification (supporting information Figure S15). Near the surface, the OA is found to be a 50/50 mixture of POA and OOA. At these altitudes the POA is dominated by BBOA and OOA is ~60% MO-OOA. The H/C and O/C vertical profiles (Figure 2d) show that OA near the surface is substantially oxidized, with an O/C~0.65. As altitude increases, OA tends to be more oxidized. This increase in oxidation with altitude may be explained by (a) fresh emissions being oxidized (leading to SOA formation and heterogeneous oxidation of POA) as they loft to higher altitudes; (b) as fresh emissions loft, they are mixed into more aged air; or (c) more likely some combination of both.
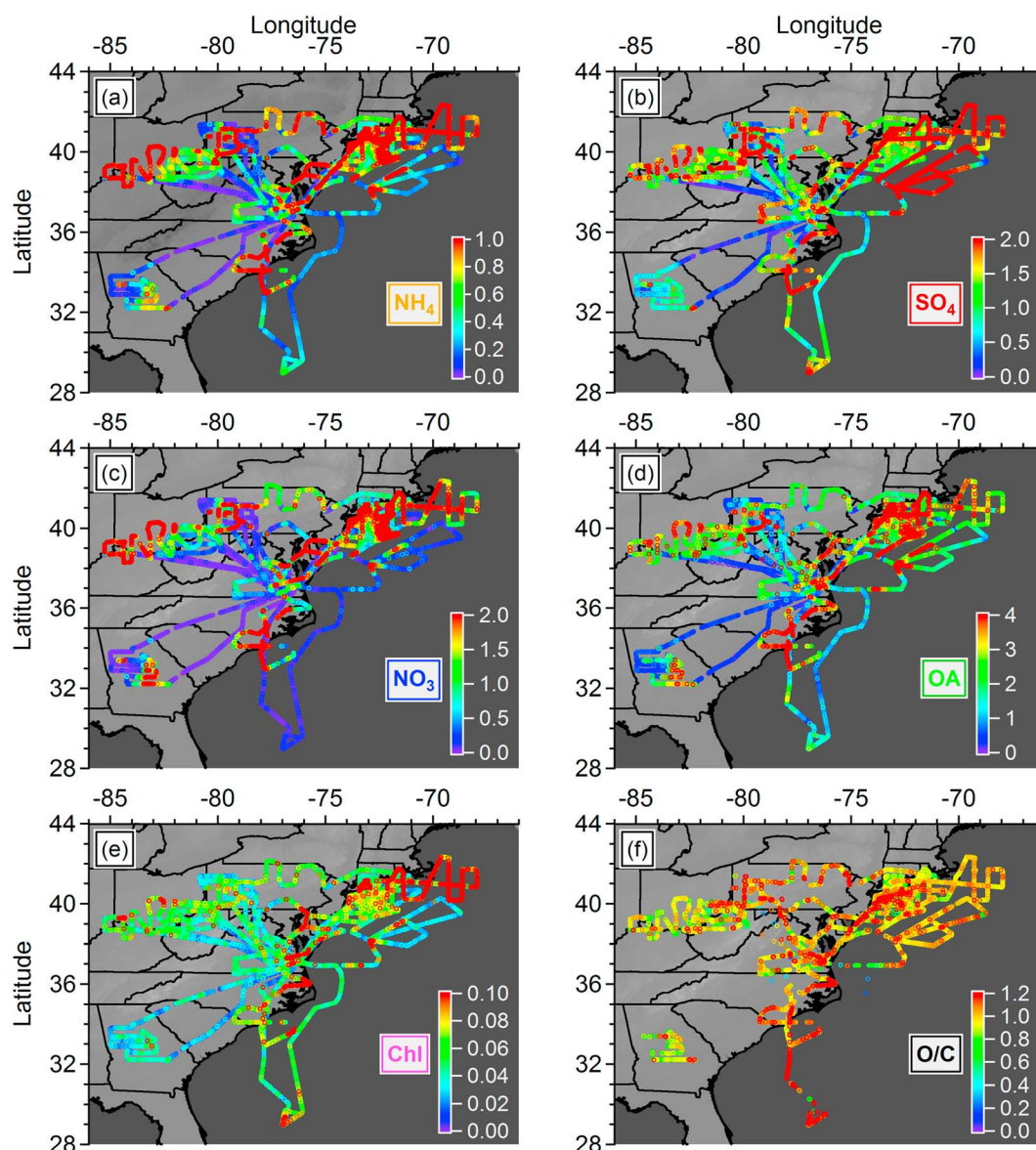
Figure 3. Spatial patterns in concentration for the AMS species (a) NH_4, (b) SO_4, (c) NO_3, (d) organic aerosol (OA), (e) Chl, and (f) O/C atomic ratios of OA during WINTER. Units for panels a–e are in $\mu g/sm^3$ and f are unitless. Data are sorted such that higher concentrations are shown on top of each flight track, and gaps in O/C in f are when OA is lower than its detection limit.

Summarizing the OA oxidation over the entire sampling region during WINTER, the normalized frequency distribution of O/C is presented in Figure 4b. The WINTER O/C distribution is compared to typical ranges for OA components from previous studies and to distributions from two previous U.S. aircraft studies: DC3 over the Central and southeastern United States (spring; Barth et al., 2015) and SEAC[4]RS over much of the continental United States (summer; Toon et al., 2016). Only data within the boundary layer (Figure S16) is included for each campaign. Figure S17 shows that the distributions are insensitive to the specific BLH chosen, to within a few kilometers. Surprisingly, OA is almost as oxidized in WINTER as in the previous campaigns. These results indicate a substantial contribution of SOA to OA during WINTER (see section 3.1.3.), in agreement with the interpretation of PMF results, despite the slower photochemistry. DC3 and SEAC[4]RS also had significant impacts from biomass burning POA (~1/4 of the OA; Liu et al., 2016; Saide et al., 2015; Yang et al., 2015), which is more oxidized than HOA (e.g., Aiken et al., 2008; Canagaratna et al., 2015). Therefore, the presence of BBOA during WINTER could not explain these data if SOA was not a major component during WINTER.
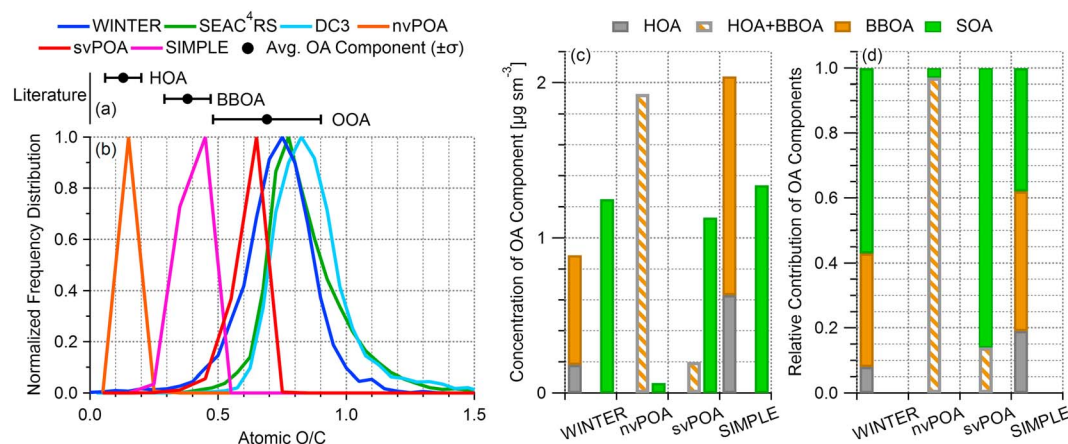
Figure 4. (a) Average and one standard deviation of O/C for hydrocarbon-like organic aerosol (HOA), biomass burning OA (BBOA), and oxidized OA (OOA) compiled in the supporting information of Canagaratna et al. (2015) are shown for reference. (b) Normalized O/C distributions for the Wintertime INvestigation of Transport, Emissions, and Reactivity (WINTER) campaign and three different simulations from GEOS-Chem using the NEI-2011 inventories with the nonvolatile primary OA (nvPOA), semivolatile POA (svPOA), and SIMPLifiEd parameterization of combustion (SIMPLE) secondary OA (SOA) formulations (only data from RF01-07 are included for these distributions). Distributions measured during the summertime SEAC⁴RS and the springtime DC3 campaigns are also shown for comparison. Only data within the boundary layer (see Figures S16 and S17) and when OA is larger than its detection limit are included in the elemental composition distributions for all campaigns (to remove the effect of noise at very low concentrations). The boundary layer height for WINTER was determined to be 0.5 km, and for both SEAC⁴RS and DC3 a value of 2 km was determined. The concentration of measured and modeled POA and SOA components are shown in c and as relative contributions in d (RF01-RF07 only).

3.1.3. Evolution of Bulk OA Composition During WINTER

The mass weighted average O/C for WINTER was 0.75. The O/C from WINTER is more oxidized than in several prior winter studies (Figure 5a). For example, an O/C of 0.35 was measured at the surface in Fresno, CA, during the month of January (Ge et al., 2012), and in Southern China an O/C was measured at 0.43 during December (Huang et al., 2013). The WINTER O/C data indicates that the OA is even more oxidized than found in a few summertime studies in a similar region to WINTER. For example, Sun et al. (2011) measured OA at Queens College, NYC, during July and found an O/C of 0.46 and Zhang found an O/C in Upton, NY, of 0.61 (Chen et al., 2015). At the summer ground-based study of Sun et al. (2011), the fraction of chemically reduced POA components (HOA and cooking OA) was 30%, compared to 9% in our study. BBOA, a more oxidized POA, was not reported by Sun et al., but accounts for 32% of the OA in our study, which contributes to the observed differences.

The atomic ratios of H/C and O/C can be plotted against each other (Figure 5a) in a Van Krevelen (VK) diagram (Van Krevelen, 1950), which is useful to visualize the evolution of OA (Hayes et al., 2013; Heald et al., 2010; Ng et al., 2010, 2011). Different slopes on the VK diagram may be due to different oxidation mechanisms or result from sampling a variable mixture of POA and OOA. A linear fit to the WINTER VK diagram yields a slope of −0.85, which is approximately consistent with the formation of carboxylic acids or hydroxycarbonyls. Chen et al. (2015) recently synthesized numerous campaigns into VK space for a range of different locations (aircraft, remote/rural, urban, and downwind sites). Air masses sampled during WINTER were predominantly urban and downwind targets. The average slopes calculated, from data summarize by Chen et al. (2015), for urban sites was −0.87 and for downwind sites was −0.86, very similar to the WINTER slope. Average data for different components and several other winter studies are also shown on Figure 5a for reference.

Ng et al. (2010, 2011) utilized the fractions of integrated signal in the AMS at m/z 44 (mostly CO_2^+) versus m/z 43 (mostly $C_3H_7^+$ from POA and $C_2H_3O^+$ from OOA) to the total OA signal as a simpler way to characterize the evolution of OA to OOA, which can also be performed with the now ubiquitous Aerosol Chemical Speciation Monitors (Ng et al., 2011). The WINTER data (Figure 5b) are consistent with Ng et al. (2010, and references within), in that they fall within a region well defined by a triangle and that most of the data lie within the defined range of mixed POA/OOA, extending into the MO-OOA area. The fraction of data, in WINTER, within the HOA region is very small, which is consistent with the low average fraction of HOA calculated with PMF (~9%).

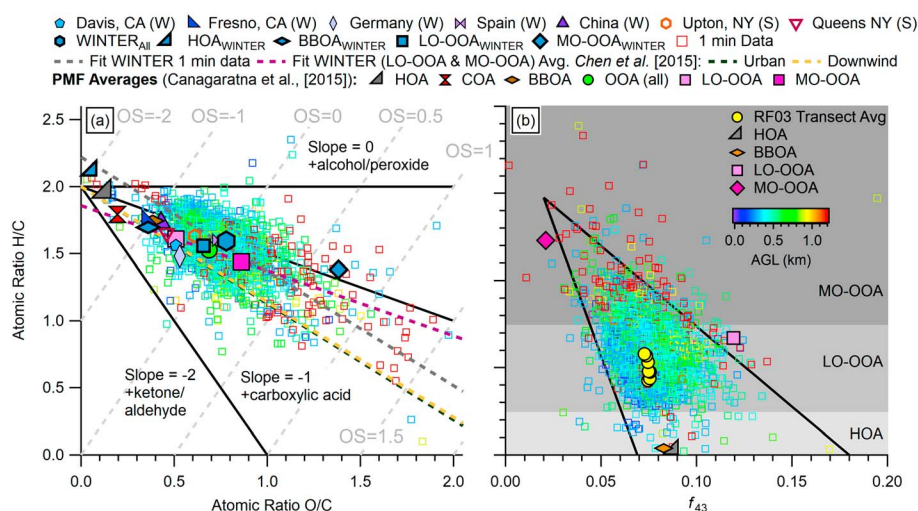**Figure 5.** (a) Van Krevelen (VK) diagram and (b) f_{44} versus f_{43} plot for 1-min data colored by altitude (above ground level [AGL]) for the entire Wintertime INvestigation of Transport, Emissions, and Reactivity (WINTER) study. Shown for reference on a are average hydrocarbon-like organic aerosol (HOA), biomass burning OA (BBOA), less-oxidized, oxidized OA (LO-OOA), and more-oxidized, oxidized OA (MO-OOA) from WINTER along with the same species plus cooking OA (COA) and total OOA summarized in Canagaratna et al. (2015) Table S1 (and references within). Also shown for comparison are data from several other wintertime studies (W in legend); Davis, CA (Chen et al., 2015), Fresno, CA (Ge et al., 2012), Melpitz, Germany (Poulain et al., 2011), Barcelona, Spain (Mohr et al., 2012), China (Huang et al., 2013), and two summertime studies (S in legend) that took place in Queens, NY (Sun et al., 2011), and Upton, NY (Chen et al., 2015). All the older studies have been corrected using the updated H/C and O/C calibrations of Canagaratna et al. (2015). Linear fits for the WINTER data (slope = −0.85), WINTER LO-OOA and MO-OOA (slope = −0.49), and the average urban (slope = −0.87) and downwind (slope = −0.86) from Chen et al. (2015) are also shown on a. In b, regions of OA oxidation, based on the observations by Ng et al. (2010), are shown in the shaded boxes, and the average f_{44} and f_{43} data from each OA component for RF01-07, as well as for each transect during RF03.

Cubison et al. (2011) proposed a plot of f_{44} versus f_{60} as useful to investigate the presence and chemical evolution of BBOA. f_{60} is the fraction of integrated signal in the AMS at m/z 60 to the total OA signal and is typically dominated by the $C_2H_4O_2^+$ ion (under biomass burning-dominated conditions), which originates from levoglucosan and related species (cellulose pyrolysis products). In WINTER, there is some evidence (Figure S18) that other ions not typically associated with biomass burning are present at m/z 60 in appreciable amounts. Therefore, to more accurately investigate the evolution of BBOA during WINTER, we plot the dominant ions f_{CO2+} and $f_{C2H4O2+}$ in Figure S19a. This shows that there is a large portion of data that is greater than a background line of non-BBOA sources of ~0.3% (Cubison et al., 2011), consistent with the conclusion that there is a ubiquitous regional source of BBOA mixed with other sources. Results from the OA source apportionment analysis (Figure S12), indeed confirms this conclusion, as the time series data of the fraction of BBOA is consistently >10% and on average is 33% of the OA mass. Some BBOA may age into OOA (Cubison et al., 2011), although the contribution of this evolution for our case study (section 3.2) appears to be small.

In addition to the above characteristic plots, Hu et al. (2015) examined the relationship of f_{CO2+} versus f_{C5H6O+} to explore the evolution of SOA production from low-NO_x isoprene oxidation. Given that this study took place during the winter, when deciduous trees have lost their leaves and the solar irradiance is reduced, the mass contribution to OA from biogenic sources is expected to be negligible (Budisulistiorini et al., 2016). A plot of WINTER data of f_{CO2+} as a function of f_{C5H6O+} (Figure S19b) clearly shows that this is the case; as the majority of the data tends to scatter around the 0.0175% background level determined for urban + biomass burning influenced air (Hu et al., 2015).

3.1.4. Comparison of OA Components and Oxidation to GEOS-Chem

The O/C distribution is also compared in Figure 4b to model results from three simulations of GEOS-Chem using the nvPOA, svPOA, and SIMPLE SOA formulations (see supporting information section S2.4 for details on this analysis). Using the nonvolatile default SOA formulation in GEOS-Chem v10-01 (nvPOA) and the 2011 NEI emissions result in an O/C mode of ~0.15, which is an underprediction of the measured peak O/C

by about a factor of 5. The nvPOA results in a POA concentration that is more than 2× greater than the measured HOA + BBOA (since BBOA is not tracked separately from POA in nvPOA and svPOA) and accounts for 97% of the total OA in this simulation (Figures 4c and 4d and supporting information Table S7). The unrealistically low production of SOA (18× too low) and high POA by this model version explains the very large underprediction of O/C.

In contrast, the svPOA simulation yields an O/C mode of 0.65, which is much closer to the observations. In this case, the concentration of POA is about 1/3 of the measurements (HOA + BBOA). The relative contribution of SOA (86%) is about 1.4× greater than measured (58%), despite being ~10% lower in concentration. This large fraction of SOA leads to better agreement with the observed O/C, albeit partially due to cancellation of errors. The SIMPLE formulation results in an O/C mode of 0.45, which falls between the nvPOA and svPOA O/C modes, and underpredicts the observations by a factor of 1.6. Here the concentration of POA (which is simulated similarly to the nvPOA case) is greater than the observations by ~2×, resulting in a lower relative SOA contribution than measured.

Summarizing these results indicates that (1) using the default nvPOA formulation is clearly inadequate at capturing the production of SOA in polluted air and use of this formulation should be avoided in future studies (either winter or summer); (2) the default svPOA formulation more closely predicts the extent of OA oxidation, reasonably predicts SOA, but significantly underestimates POA; and (3) the less computationally expensive SIMPLE formulation performs reasonably well at reproducing the mass concentration of SOA, although it overpredicts POA (presumably due to too high POA emissions in NEI2011). We therefore recommend using the SIMPLE or svPOA formulations in GEOS-Chem in the future. In addition, a reduction in O/C for primary OA and an increase in O/C for secondary OA, using the SIMPLE formulation, better predicts the extent of oxidation in this formulation (Figure S21) and should be considered when evaluating wintertime OA oxidation in other regions.

3.2. Wintertime Evolution of OA: A Case Study Downwind of the NYC Metropolitan Area

Several studies have investigated the production and downwind evolution of urban SOA (de Gouw et al., 2008; DeCarlo et al., 2010; Hayes et al., 2013; Kleinman et al., 2007, 2008), but most of these studies were conducted during warmer seasons (e.g., spring or summer). To investigate these processes during winter, the NYC metropolitan area sampled during RF03 (7 February 2015) was selected as a case study. The portion of the flight path, for this case study, followed a pseudo-Lagrangian pattern heading east of NYC. This flight was selected because the flight path was predominantly off the coast of the northeastern seaboard, and as anthropogenic emissions essentially stop at the coastline, the plume sampled is dominated by advection, dilution, and aging of urban emissions from metro NYC, thus providing a unique case to investigate the formation and evolution of SOA during winter. The relevant portion of the flight path for this analysis is shown in Figure 6a. The average wind direction during this time was southwesterly at 225° and with an average speed of 7 m/s, and the flight path crossed the metro NYC plume several times. Based on the flight path, wind direction, and time series concentration profiles (Figure 6c), five plume transects were identified as T1–T5. Although the plane crossed the plume two more times downwind of T5, these transects showed strong evidence of mixing from unrelated air masses and therefore were excluded in this analysis. All gas-phase species mixing ratios increased as the aircraft entered a plume transect and decreased to background levels upon exiting the transect. This, along with the average wind direction, strongly suggests that we were sampling NYC urban emissions injected into a regional background. To confirm this, 48-hr FLEXPART back trajectories (section 2.2.1) are shown in Figures 6a and 6b and supporting information Figure S22. All back trajectory altitude profiles show slight uplift approximately 12 hr prior to the air masses descending to the point of the aircraft transect. The back trajectories for T1 and T2 pass directly through NYC, whereas T3–T5 show the air coming from the northern metropolitan area. The average hourly surface (<140 m) CO, simulated in GEOS-Chem, is also overlaid on the map (Figure 6a) and represents the areas impacted by urban emissions in the area. All back trajectories distinctly cross a region of high CO emissions, further indicating that all transects sampled were directly influenced by metro NYC urban emissions. In addition, based on transport times determined from the back trajectories (see section 3.2.1), the amount of transport during daylight ranged from 3 to 10 hr for T1 and T5, respectively (supporting information Table S8).

OA/ΔCO can be used as a metric for evaluating the evolution of OA in an urban plume, where ΔCO is a conserved tracer used to account for dilution of primary emissions. The method allows quantifying the increase
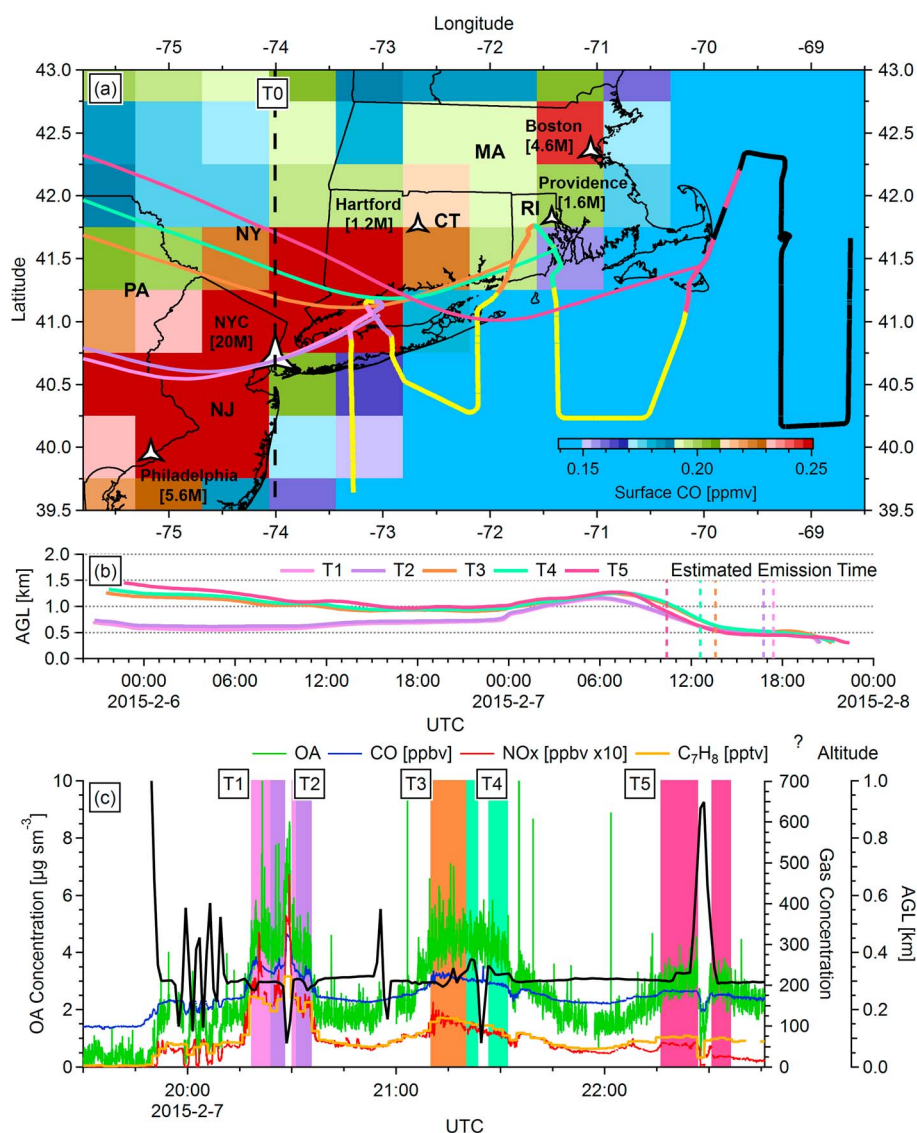
Figure 6. (a) Map of the flight track for RF03 colored by day (yellow) and night (black), according to sunrise/sunset, and median 48-hr FLEXPART back trajectories colored by transect number. Overlaid on a is the GEOS-Chem (NEI-2011) CO, which is the modeled average hourly surface CO (<140 m) concentrations, from 10:00 to 23:00 UTC (i.e., from the estimated emission time to the end of sampling of T5). Also shown on the map are cities and populations (in millions) for reference. (b) Altitude profiles of the median FLEXPART back trajectories (colored by transect number), along with the estimated time of emission (determined from linearly interpolating across the T0 line shown in a for each transect). (c) Time series data of organic aerosol (OA), CO, toluene, NO_x, and flight altitude for the relevant period of RF03. Transects T1–T5 are colored uniquely and identified in the legend in b. The 25th and 75th percentiles for all back trajectories and altitude profiles are not shown here for clarity (see supporting information Figure S22). AGL = above ground level.

in OA/ΔCO (i.e., ΔOA/ΔCO) with photochemical age due to SOA formation (e.g., DeCarlo et al., 2010; Docherty et al., 2008; Hayes et al., 2013; Kleinman et al., 2007, 2008; Ortega et al., 2016; Takegawa et al., 2006). As mentioned above, Figure 6c suggests that there is a relatively constant OA baseline of ~1.6 µg/sm³, indicating that the NYC plume is emitted into a preexisting regional background. Therefore, each of the plume transects in this case study were analyzed for the ratio of $\Delta X_{Species}$/ΔCO, where $\Delta X_{Species}$ = total $X_{Species}$ − regional background $X_{Species}$. Those ratios represent the impact of metro NYC emissions.

Figure 7a shows the evolution of ΔOA/ΔCO, which shows an increasing trend from T1 to T5. To evaluate the causes of the increases, the decay of the measured aromatic VOCs were similarly analyzed (Figure 7d and supporting information Figure S23), since aromatic VOCs are thought to be significant contributors to urban SOA
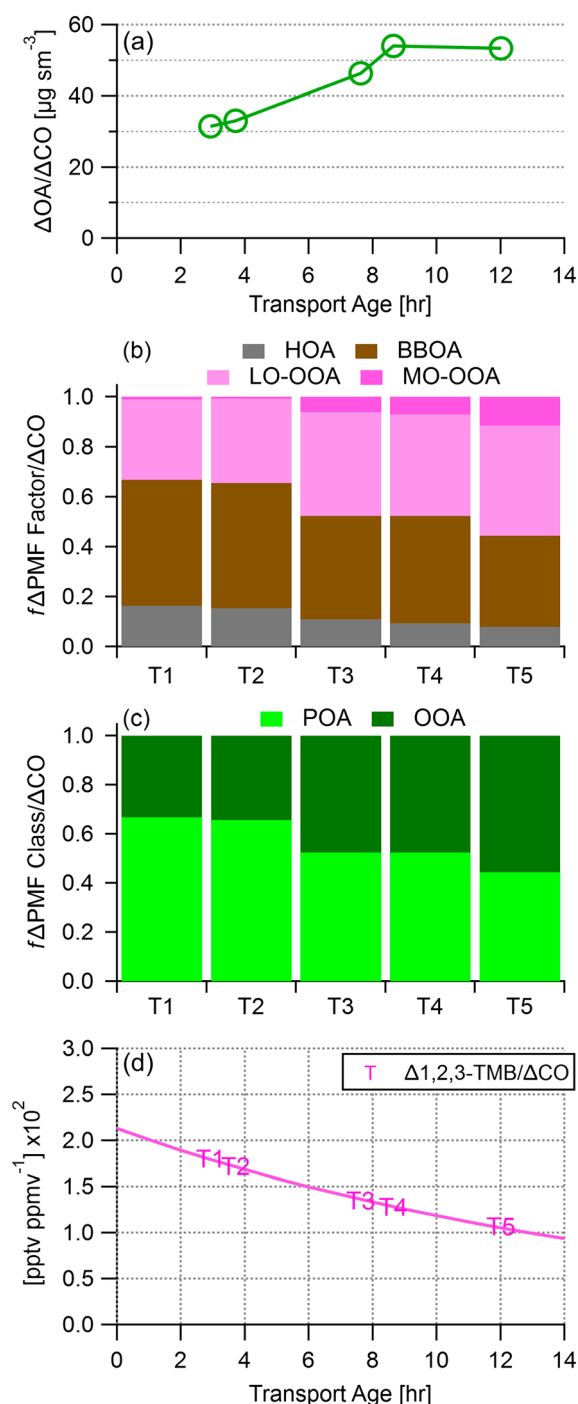
Figure 7. (a) Evolution of ΔOA/ΔCO, (b, c) the fraction of organic aerosol (OA) components from positive matrix factorization (PMF) analysis, and (d) decay of an example volatile organic compound (see Figure S23 for all volatile organic compound ratios) used for estimating photochemical age. The standard errors for the y variables in a and d are smaller than the data points shown. BBOA = biomass burning OA; HOA = hydrocarbon-like OA; LO-OOA = less-oxidized, oxidized OA; MO-OOA = more-oxidized, oxidized OA (MO-OOA); POA = primary organic aerosol.

formation (Hayes et al., 2015; Odum et al., 1997). As the evolution of the plume progressed from T1 to T5, all aromatic ΔVOC/ΔCOs (with the exception of the least reactive benzene) decreased as ΔOA/ΔCO increased, which is consistent with photochemical aging and thus should lead to SOA formation.

To investigate the causes of OA evolution, PMF results are shown in Figures 7b and 7c. The fraction of OOA increased from T1 (33%) to T5 (56%). Even at T5, this fraction is lower than what was reported by de Gouw et al. (2005) and Kleinman et al. (2007; 57–75%) in the Northeastern Air Quality Study (NEAQS) 2002 study, which also took place in the NE-US but during the summer. During the same study de Gouw et al. (2005) reported that only 11% of the OA mass was from anthropogenic primary sources, which is significantly lower than the POA at T1 (67%) or even T5 (44%). The larger fraction of POA measured in this study is driven by the large fraction of BBOA, attributed to residential wood burning, which was absent from the 2002 summertime study, as well as the absence of biogenic OA during WINTER (which was very likely an important contributor to the summer study). The progression of OA components from T1 to T5 shows that the fraction of primary components decreased over time and the OOA components increased as the air was photochemically aged, consistent with many previous studies (de Gouw et al., 2008; DeCarlo et al., 2010; Hayes et al., 2013; Kleinman et al., 2007, 2008). The increase in SOA fraction is predominately a result of gas-to-particle conversion since the POA remained relatively constant throughout these transects (see Figure 8b). This suggests that aging of BBOA into OOA (Cubison et al., 2011) played a minor role during this case study.

This study took place during the winter, where clouds can be prevalent. The evidence for SOA formation in clouds is mixed (Ervens, 2015; Gilardoni et al., 2016; Wagner et al., 2015) but cannot be discounted. Vertical profiles of ambient temperature and relative humidity (RH) were constructed from data collected at two nearby sounding sites, OKX (40.87°N, 72.87°W, near T1/T2) and CHH (41.67°N, 69.97°W, near T5) at 0 UTC and 12 UTC (Figure S24). These data indicate that at the average aircraft altitude (0.3 km, pressure Altitude) during RF03 (and up to 2 and 3 km), RH was persistently below 100%. The time series of ambient RH and air temperature (Figure S25) measured from the aircraft, during the relevant portion of RF03, as well as forward facing camera images from the C-130 taken at roughly the middle of each transect from T1 to T5 (Figure S26) confirm that we were not flying directly in clouds and that the RH was <100% during all plume transects. Three of four nearby airports (John F. Kennedy, NY; Islip/Macarthur, NY; Montauk, NY; and Nantucket Memorial, MA) reported trace amounts of precipitation (Local Climatological Data, 2018) at some point during the sampling period. Furthermore, during these transects, there was no evidence of a significant increase in sulfate (Figure S27) as one would expect if aqueous phase chemistry was a substantial factor (Ervens, 2015, and references within). These data combined suggest that wet deposition and cloud processing were most likely insignificant contributors (but cannot be completely excluded) to the production or loss of SOA in this case study.

3.2.1. Air Mass Age

To enable a quantitative analysis of the rate of SOA formation, the age of the air (since injection of urban emissions into the NYC metropolitan area) for each transect was estimated based on both the transport time and
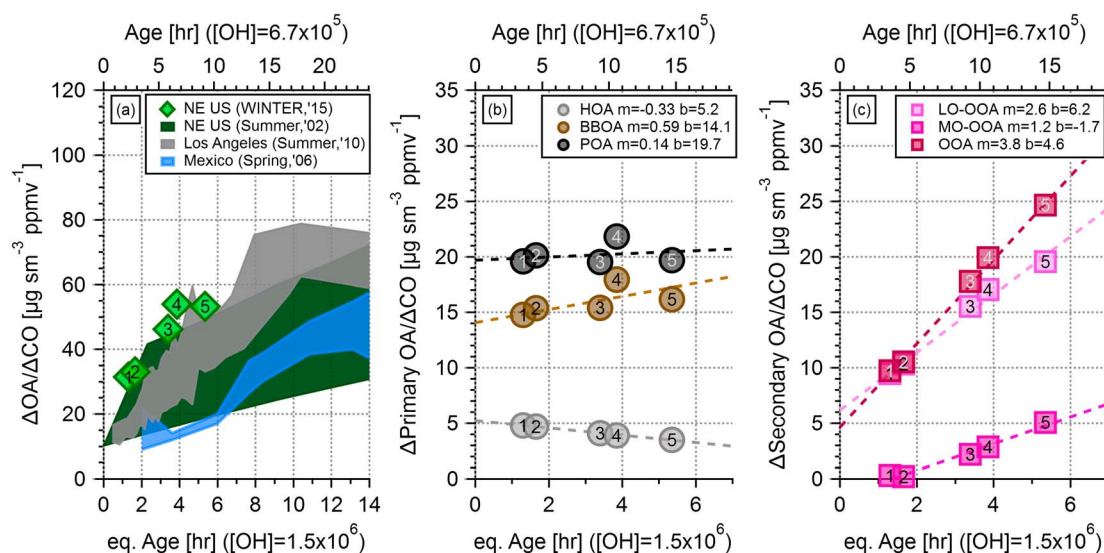
Figure 8. (a) RF03 plume transect $\Delta OA/\Delta CO$ versus photochemical age using an standardized OH (bottom x axes) of 1.5×10^6 molecules per cubic centimeter (for ease of comparison to literature studies) and the estimated OH during our study of 6.7×10^5 molecules per cubic centimeter (top x axes). Shown for comparison are $\Delta OA/\Delta CO$ values measured in the northeastern United States (NE-US) during summer (NEAQS-2002; de Gouw et al., 2005; DeCarlo et al., 2010; Kleinman et al., 2007), Los Angeles in summer (CalNex; Hayes et al., 2013; Ortega et al., 2016), and Mexico in spring (MILAGRO-2006) (DeCarlo et al., 2010; Kleinman et al., 2008). For a complete discussion on the comparison studies see supporting information section S2.5.1. $\Delta Factor/\Delta CO$ for (b) primary organic aerosol (POA) components and for (c) secondary organic aerosol (SOA) components are also shown with linear fits, where "m" and "b," in the legend, denote the slope and intercept, respectively, using the bottom x axes. Note, the standard errors for the y variables for all WINTER data in a–c are smaller than the data points shown. A small apparent increase in biomass burning organic aerosol (BBOA) with age may be due to noise or to small variations in BBOA emissions with time of day. HOA = hydrocarbon-like OA; LO-OOA = less-oxidized, oxidized OA; MO-OOA = more-oxidized, oxidized OA.

photochemical processing. The transport age is described as the average amount of time the air mass took to travel to each point along the transect's flight path, from a defined time zero (T0), which was chosen as the longitude of NYC Center, and is shown on Figure 6a. For comparison, the transport age calculated based on the average wind speed, measured from onboard the aircraft at each transect, and distance from NYC was within 8% of the transport age determined using FLEXPART. To evaluate the amount of chemical processing of the air mass intercepted in each transect, photochemical ages were estimated using three different methods: (1) VOC ratio clock, (2) the NO_x clock, and (3) a novel approach to the VOC ratio clock, termed the VOC/CO clock. We note that CO formation from VOCs is a very small contributor to its concentrations in urban plumes (Griffin et al., 2007). The first two methods have been described at length in previous literature (de Gouw et al., 2005; Kleinman et al., 2003, 2007, 2008; Olszyna et al., 1994; Parrish et al., 2007) and are only briefly described here. All three methods are based on the first-order decay of a species under OH oxidation (equation (1)).

$$Y_{t=t} = Y_{t=0}\exp^{-kt[OH]} \tag{1}$$

where Y_i is the concentration of any OH reactive species i, t is time, k is the rate constant for a given species with OH, and the subscript $t = 0$ ($t = t$) denotes Y_i at the time of emission (aircraft measurement).

The VOC ratio clock is based on the concept that if two VOCs are coemitted from a given source with a characteristic initial emission ratio, the more reactive VOC will be removed faster from the atmosphere, through oxidation, as the air moves downwind. As a result, any ratio of VOCs (VOC_a/VOC_b), where the more reactive VOC is in the numerator, will decrease with time and can be substituted in equation (1) for Y. The rate constant for a ratio of VOCs is represented by the difference, or $k_{(VOCa-VOCb)}$. The VOC/CO clock is identical to the VOC ratio clock except CO is used in the denominator. On timescales relative to VOCs, CO is considered inert ($k_{OH, VOCi} >> k_{OH, CO}$) thus, $k_{OH, CO} \approx 0$, and only $k_{OH, VOCi}$ is needed for this method.

Table 1
Estimated OH and Initial Emission Ratio (eER) Determined for Each Pair of Species (Figure 7d and supporting information S23)

Pairs of species	OH × 10^5 (molecules per cubic centimeter)	eER	k_{OH} × 10^{-12} (cubic centimeter per molecule per second)
Δ1,2,3-TMB/Δtoluene	5.3	0.09	26.3
Δ1,2,4-TMB/Δtoluene	5.4	0.09	26.1
Δ (m,p-xylene+ethylbenzene)/Δtoluene	6.6	0.62	6.5
Δo-xylene/Δtoluene	3.3	0.17	7.2
Δ1,2,3-TMB/Δo-xylene	6.0	0.53	19.1
Δ1,2,4-TMB/Δo-xylene	6.1	0.53	18.9
Δtoluene/ΔCO	13	1455[a]	6.37
Δ1,2,3-TMB/ΔCO	5.0	213[a]	32.7
Δ1,2,4-TMB/ΔCO	6.8	131[a]	32.5
Δ (m,p-xylene+ethylbenzene)/ΔCO	9.8	906[a]	12.9
Δo-xylene/ΔCO	7.9	249[a]	13.6
ΔNO$_x$/ΔNO$_y$	5.0	1	6.79
Average OH	6.7 (±2.6)		

Note. The average OH (±1σ) and the OH rate constant (k_{OH}) used are also shown. k_{OH} for toluene and NO$_x$ were calculated at the average temperature of the plume transects (269 K), and all other k_{OH} are temperature independent (Calvert et al., 2015).
[a]Units of pptv/ppmv.

The NO$_x$ clock is defined such that at the time of emission (i.e., t = 0) NO$_y$ = NO$_x$. Therefore, as air is transported away from the source, the ratio (NO$_x$/NO$_y$) will decrease and can also be substituted in equation (1) for Y. Since, in this method, the main loss process of NO$_x$ is assumed to be photochemically driven from the reaction of OH with NO$_2$, k is simply that of NO$_2$ with OH. The impact of nighttime N$_2$O$_5$ chemistry is more important at T5 and may reduce the accuracy of the NO$_x$ clock for this transect.

For all three methods described, equation (1) can be used to determine the photochemical age (t) or the concentration of OH. In this analysis, 13 ratios (Δ1,2,3-TMB/Δtoluene; Δ1,2,4-TMB/Δtoluene; Δ1,2,3-TMB/Δ o-xylene; Δ1,2,4-TMB/Δo-xylene; Δ (m,p-xylene+ethylbenzene)/Δtoluene; Δo-xylene/Δtoluene; Δtoluene/ ΔCO; Δo-xylene/ΔCO; Δ (m,p-xylene+ethylbenzene)/ΔCO; Δ1,2,3-TMB/ΔCO; Δ1,2,4-TMB/ΔCO; and ΔNO$_x$/ ΔNO$_y$) were evaluated by fitting versus transport time to estimate OH (Figures 7d and S23), since no direct measurement of OH was available during WINTER. Here OH is assumed to be the dominant daytime oxidant available for reaction with the precursor VOCs and NO$_x$ during atmospheric transport. In NEAQS-2002 Warneke et al. (2004) investigated VOC oxidation, by O$_3$, NO$_3$, and OH, and found that anthropogenic and oxygenated VOCs were primarily oxidized during the daytime by OH. During winter, OH is expected to be lower than in the summer due to (a) reduced water vapor decreasing the fraction of O(^{1}D), which converts to OH, and (b) decreased photolysis of OH precursors such as O$_3$ as a result of reduced solar radiation (Gligorovski et al., 2015; Heard et al., 2004; Ren et al., 2006). However, the potential importance of the radical precursors ClNO$_2$, HONO, and CH$_2$O during WINTER may lead to larger OH concentrations than expected otherwise (Heard et al., 2004). Based on our analysis, the average daytime OH was estimated to be 6.7 ± 2.6 × 10^5 molecules per cubic centimeter (Table 1), which is indeed lower than typical summer average daytime OH (1.2 × 10^6–3 × 10^6 molecules per cubic centimeter; de Gouw et al., 2005; Hayes et al., 2013; Ren et al., 2006; Volkamer et al., 2006) and within a range of what has been observed in previous winter studies (1.1 × 10^5–7 × 10^5 molecules per cubic centimeter; Berresheim et al., 2013; Emmerson et al., 2005; Heard et al., 2004; Ren et al., 2006). Our estimated OH is also consistent with a mean daytime OH of 8 × 10^5 molecules per cubic centimeter for the GEOS-Chem simulations of WINTER.

To enable a direct comparison to results of prior publications that mostly used a standardized OH concentration of 1.5 × 10^6 molecules per cubic centimeter (Hayes et al., 2013; Hu et al., 2016; Mao et al., 2009; Ortega et al., 2016; Palm et al., 2016), we used this value to determine equivalent (eq.) ages using equation (2) as follows:

$$\text{eq.Age} = \text{transport time} \times \frac{[OH]_{\text{estimated}}}{[OH]_{\text{standard}}} \tag{2}$$
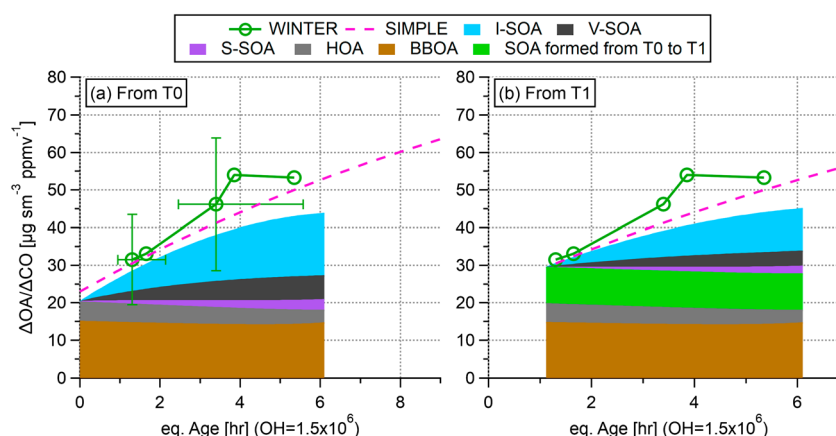
Figure 9. Comparison of measured to predicted secondary organic aerosol (SOA) formation from the box model, with unscaled primary intermediate volatility organic carbons. Model simulations were initialized at (a) time zero (T0) and (b) Transect 1 (T1). SOA formed from T0 to T1 is the amount of measured LO-OOA + MO-OOA at T1. The SIMPLE parameterization of urban SOA (Hayes et al., 2015) is also shown for comparison. In the figure legend I-SOA is SOA from primary intermediate volatility organic carbons, V-SOA is SOA from volatile organic compounds, and S-SOA is SOA from primary semivolatile volatility organic carbons. The y-error bars in a represent the uncertainty of the OA and CO measurements, and the x-error bars show the uncertainty in equivalent age as a result of the uncertainty in estimated OH concentration. Only two error bars are shown for clarity. BBOA = biomass burning OA; HOA = hydrocarbon-like OA; LO-OOA = less-oxidized, oxidized OA; MO-OOA = more-oxidized, oxidized OA.

3.2.2. Wintertime Evolution of SOA

The average $\Delta OA/\Delta CO$ versus equivalent photochemical age for the case study are shown in Figure 8a. As in previous field studies (e.g., DeCarlo et al., 2010; Hayes et al., 2013), $\Delta OA/\Delta CO$ increases steeply with age. For comparison, Figure 8 also shows results from summertime measurements in Los Angeles during CalNex (Hayes et al., 2013; Ortega et al., 2016), summer NE-US from the NEAQS-2002 study (de Gouw et al., 2005; DeCarlo et al., 2010; Kleinman et al., 2007), and springtime in Mexico City (MILAGRO; DeCarlo et al., 2010; Kleinman et al., 2008). The $\Delta OA/\Delta CO$ in WINTER reaches ~32 $\mu g \cdot sm^{-3} \cdot ppmv^{-1}$ in about 1 eq. hr of aging at T1 and steadily increases to ~54 $\mu g \cdot sm^{-3} \cdot ppmv^{-1}$ after about 5 eq. hr of aging by T5, indicating an SOA formation rate of 4 $\mu g \cdot sm^{-3} \cdot ppmv^{-1} \cdot eq. hr^{-1}$. For comparison, the average rate of formation in the NE-US summer was observed to be ~3 $\mu g \cdot sm^{-3} \cdot ppmv^{-1} \cdot eq. hr^{-1}$, ~6 $\mu g \cdot sm^{-3} \cdot ppmv^{-1} \cdot eq. hr^{-1}$ in Los Angeles summer, and ~5 $\mu g \cdot sm^{-3} \cdot ppmv^{-1} \cdot eq. hr^{-1}$ in Mexico City spring. The formation rate has been observed to be steeper at short ages and eventually plateaus at ages of ~1 day (Hodzic & Jimenez, 2011; Ortega et al., 2016). Overall, the WINTER results show that urban SOA formation is proceeding with similar intensity and rate as during summer studies, once oxidant and emission/dispersion differences are accounted for.

The primary OA components (HOA, BBOA, and total POA) and oxidized components (LO-OOA, MO-OOA, and total OOA) are analyzed identically to OA in Figures 8b and 8c. HOA and BBOA show nearly constant levels, as does total POA, which is consistent with the identification as primary components, the good pseudo-Lagrangian approximation of the case study, and their slow aging due to heterogeneous oxidation (e.g., DeCarlo et al., 2008; Ortega et al., 2016). OOA (Figure 8c) clearly captures nearly all the increase in OA with photochemical age, which is consistent with SOA production. Total OOA increases at a rate of 3.8 $\mu g \cdot sm^{-3} \cdot ppmv^{-1} \cdot CO$ eq. hr^{-1}. These results further corroborate the efficient wintertime production of SOA observed in the NYC metro area.

3.2.3. SOA Production in Pseudo-Lagrangian Study: Measurements Versus Box Model

A box model (Hayes et al., 2015; Ma et al., 2017) was used to simulate the formation of SOA in the NYC metro case study (Figure 9). The box model was simulated with two different initializations: (1) from T0 (Figure 9a, referred to as I_{T0}) by using the estimated initial emission ratios from the fits shown in Figure S23 and (2) from T1 (Figure 9b, referred to as I_{T1}), in which all SOA formed before T1 is accounted for by the measured average OOA at T1. Additionally, I_{T0} and I_{T1} were run with two cases for P-IVOC inputs: (a) constrained using the CalNex measurements of Zhao et al. (2014) and (b) scaled down according to the ratio of measured VOCs between WINTER and CalNex (see supporting information section S1.4).

The unscaled P-IVOC results (Figure 9) more closely reproduce the measured results, when compared to the scaled P-IVOCs (Figure S29), suggesting that the VOCs and P-IVOCs have dominant contributions from different sources. This is consistent with Zhao et al. (2014), who attributed P-IVOCs to non-on-road sources, and McDonald et al. (2018), who showed that volatile chemical products (e.g., personal care and cleaning products, coatings, adhesives, or pesticides) are major sources of P-IVOCs. Results from both initializations (with unscaled P-IVOCs, Figure 9) are consistent and capture ~2/3 of the observed SOA formation (I_{T0} is within 63%, and I_{T1} is within 60% of the observed SOA formation, on average over the sampling period). This model was also lower by a very similar amount (~53%, see supporting information Figure S30) than the observations for the same range of short photochemical ages in the Los Angeles case (Ma et al., 2017). This persistent result suggests that some fast-reacting precursors might be missing or that the SOA formation chemistry of SVOCs and P-IVOCs are faster than implemented in these parameterizations, for example, if fast autoxidation reactions played a role (Crounse et al., 2013), although this is less likely under colder winter temperatures.

Similar to what has been observed in CalNex, the fraction of the total SOA formed from VOCs (according to the model) is ~25–30%. However, during WINTER, the fractional contribution to SOA from SVOCs is ~3× less, whereas SOA from P-IVOCs is about 2× greater than what was observed in summertime LA, after ~6 hr of photochemical aging. Lower SOA from SVOCs is consistent with lower temperatures driving the SVOCs to the particle phase where they remain as POA. Similarly, P-IVOCs more rapidly condense to form SOA at these temperatures, thus increasing their relative contribution at younger ages (together with their higher relative input concentrations for the default model case).

The box model was also used to simulate O/C during this case study for each of the four initializations (see supporting information section S1.4 and Figure S32). All four simulations capture the general trend of increasing O/C with age observed but are consistently on the low end of the uncertainty range of the measured O/C.

In addition to the box model, the SIMPLE parameterization (Hayes et al., 2015; Hodzic & Jimenez, 2011; Kim et al., 2015), with the parameters derived by Hayes et al. (2015) for Los Angeles (Figure 9), is also consistent with the observed SOA formation, albeit slightly lower (~80% of observed amount at T5). This result suggests that the parameters derived from Los Angeles region in summertime can also be used to reasonably predict the SOA formation from NYC in winter. Again, the ratio of the SIMPLE parameterization to the observations is very similar to the Los Angeles results for the same range of short photochemical ages.

Unfortunately, the range of photochemical ages reached in this case study was limited. Extending the I_{T0} simulation to 3 days (supporting information Figure S31) shows that both the box model and the SIMPLE parameterization plateau after ~1–2 days, due to the depletion of the precursor VOC. However, they reach significantly different final values. It is not possible to constrain the SIMPLE parameterization for longer ages in this domain with the information available to this manuscript. However, some of the air masses sampled contain air that has been oxidized for longer periods than in this case study. Thus, we recommend optimizing the SIMPLE parameters by performing multiple simulations in GEOS-Chem (or other 3-D models) and finding the ones that results in optimal agreement with the regional observations, similar to what was done by Murphy et al. (2017), who used a different 3-D model.

4. Conclusions

Wintertime ambient aerosol measurements were made aboard the NCAR C-130 in the NE-US from February to March 2015, as part of the WINTER campaign. These measurements offered a unique opportunity to investigate aerosol sources and processes during wintertime, which are understudied in the scientific literature. This manuscript focuses on (1) general trends observed in measured submicron aerosol throughout the NE-US; (2) sources and processing of submicron OA; and (3) wintertime production of SOA, through a pseudo-Lagrangian case study.

On average, the submicron aerosol concentration was 5 μg/sm^3, with 13% being NH$_4$, 22% NO$_3$, 26% SO$_4$, 1% Chl, and 37% OA. Comparing to summer measurements in a similar region, wintertime values are lower by about a factor of 2.5. However, accounting for differences in BLH between winter and summer, these results suggest that wintertime total column concentrations are significantly lower. This observation is consistent with several other studies in that wintertime concentrations tend to be approximately 20% lower, on average, than in summer, but with substantial variability (2–63%). Based on PMF analysis, primary HOA (a surrogate for

vehicle exhaust and similar sources) was a minor contributor to the overall OA mass (<10%), while BBOA was fairly ubiquitous, accounting for 33% of the OA. BBOA in this study is thought to be dominated by residential wood burning, consistent with wintertime studies in other regions. OA was also fairly oxidized, with ~60% of the OA mass apportioned to OOA, and was almost as oxidized as in recent spring and summer U.S. aircraft campaigns. The atomic O/C mode in WINTER was 0.75 (<0.5-km altitude).

SOA and O/C are significantly underestimated for the nvPOA default formulation within GEOS-Chem v10-01, which produces an O/C mode 5 times lower than the measurements, and with 97% of the OA mass as primary. The nvPOA GEOS-Chem simulation only produced a small fraction of SOA (3%), far lower than observed (~60%). This result, clearly indicates that the GEOS-Chem v10-01 formulation with nvPOA and anthropogenic SOA from benzene, toluene, and xylene (based on Pye et al., 2010) is inadequate to capture SOA formation from urban emissions, and we recommend completely avoiding its use in future studies (for either summer or winter studies). When GEOS-Chem was used with the alternative default parameterization, which includes SVOC and P-IVOC (svPOA) or the SIMPLE SOA parameterization (Hayes et al., 2015; Hodzic & Jimenez, 2011) as implemented in GEOS-Chem by Kim et al. (2015), model SOA concentrations were closer to the observations. These two parameterizations differed by about an order of magnitude for POA, with svPOA underpredicting it by a factor of 5, while SIMPLE overpredicted POA by a factor of ~2. O/C was closest to the observations for the svPOA parameterization, however, partially due to a cancellation of errors (too low POA together with too high O/C for SOA). Considering the reasonable performance of the SIMPLE SOA parameterization during WINTER and its computational efficiency, we recommend this parameterization for future GEOS-Chem studies. The svPOA parameterization should be considered for studies where additional details for SOA formation are useful.

A case study from a research flight that flew a pseudo-Lagrangian flight pattern off the coast of the NYC metropolitan area was used to investigate the production of SOA. Given that it was winter, this case study provided a unique opportunity to examine the impact of urban emissions, isolated from biogenic influences, on SOA, something that cannot be done easily during the summertime. Evolution of the ratios of different species are consistent with the pseudo-Lagragian nature of this case study, and through comparison with the transport age, allowed estimation of the concentration of OH (6.7×10^5 molecules per cubic centimeter, as expected lower than in summer), and therefore photochemical age. SOA production from urban emissions in the NE-US during winter was as efficient and rapid (when accounting for the differences in OH) as what has been observed in summer studies. This supports previous literature evidence of the importance of SOA formation from urban emissions and the need to represent this source in atmospheric models. A box model that approximately reproduced the Los Angeles observations, as well as the SIMPLE parameterization, performed well for this case study, slightly underpredicting SOA at short photochemical ages, and with consistent results with GEOS-Chem for the comparable simulations. This persistent difference may indicate that some fast-reacting precursors are missing from the model, and/or that some fast reaction pathways may be missing from the models.

References

Aiken, A. C., DeCarlo, P. F., Kroll, J. H., Worsnop, D. R., Huffman, J. A., Docherty, K. S., et al. (2008). O/C and OM/OC ratios of primary, secondary, and ambient organic aerosols with high-resolution time-of-flight aerosol mass spectrometry. *Environmental Science & Technology*, *42*(12), 4478–4485. https://doi.org/10.1021/es703009q

Allan, J. D., Alfarra, M. R., Bower, K. N., Williams, P. I., Gallagher, M. W., Jimenez, J. L., et al. (2003). Correction to "Quantitative sampling using an Aerodyne aerosol mass spectrometer: 2. Measurements of fine particulate chemical composition in two U.K. cities". *Journal of Geophysical Research*, *108*(D9), 4284. https://doi.org/10.1029/2003JD001608

Allan, J. D., Jimenez, J. L., Williams, P. I., Alfarra, M. R., Bower, K. N., Jayne, J. T., et al. (2003). Quantitative sampling using an Aerodyne aerosol mass spectrometer 1. Techniques of data interpretation and error analysis. *Journal of Geophysical Research*, *108*(D3), 4090. https://doi.org/10.1029/2002JD002358

Apel, E. C., Emmons, L. K., Karl, T., Flocke, F., Hills, A. J., Madronich, S., et al. (2010). Chemical evolution of volatile organic compounds in the outflow of the Mexico City Metropolitan area. *Atmospheric Chemistry and Physics*, *10*(5), 2353–2375. https://doi.org/10.5194/acp-10-2353-2010

Bahreini, R., Dunlea, E. J., Matthew, B. M., Simons, C., Docherty, K. S., DeCarlo, P. F., et al. (2008). Design and operation of a pressure-controlled inlet for airborne sampling with an aerodynamic aerosol lens. *Aerosol Science and Technology*, *42*(6), 465–471. https://doi.org/10.1080/02786820802178514

Bahreini, R., Ervens, B., Middlebrook, A. M., Warneke, C., de Gouw, J. A., DeCarlo, P. F., et al. (2009). Organic aerosol formation in urban and industrial plumes near Houston and Dallas, Texas. *Journal of Geophysical Research*, *114*, D00F16. https://doi.org/10.1029/2008JD011493

Bardouki, H., Liakakou, H., Economou, C., Sciare, J., Smolík, J., Ždímal, V., et al. (2003). Chemical composition of size-resolved atmospheric aerosols in the eastern Mediterranean during summer and winter. *Atmospheric Environment*, *37*(2), 195–208. https://doi.org/10.1016/S1352-2310(02)00859-2

Barth, M. C., Cantrell, C. A., Brune, W. H., Rutledge, S. A., Crawford, J. H., Huntrieser, H., et al. (2015). The deep convective clouds and chemistry (DC3) field campaign. *Bulletin of the American Meteorological Society*, *96*(8), 1281–1309. https://doi.org/10.1175/BAMS-D-13-00290.1

Berresheim, H., McGrath, J., Adam, M., Mauldin, R. L., Bohn, B., & Rohrer, F. (2013). Seasonal measurements of OH, NO_x, and J (O^1D) at Mace Head, Ireland. *Geophysical Research Letters*, *40*, 1659–1663. https://doi.org/10.1002/grl.50345

Bey, I., Jacob, D. J., Yantosca, R. M., Logan, J. A., Field, B. D., Fiore, A. M., et al. (2001). Global modeling of tropospheric chemistry with assimilated meteorology: Model description and evaluation. *Journal of Geophysical Research*, *106*(D19), 23,073–23,095. https://doi.org/10.1029/2001JD000807

Boers, R., van Weele, M., van Meijgaard, E., Savenije, M., Siebesma, A. P., Bosveld, F., & Stammes, P. (2015). Observations and projections of visibility and aerosol optical thickness (1956–2100) in the Netherlands: Impacts of time-varying aerosol composition and hygroscopicity. *Environmental Research Letters*, *10*(1), 015003. https://doi.org/10.1088/1748-9326/10/1/015003

Bond, T. C., Bhardwaj, E., Dong, R., Jogani, R., Jung, S., Roden, C., et al. (2007). Historical emissions of black and organic carbon aerosol from energy-related combustion, 1850–2000. *Global Biogeochemical Cycles*, *21*, GB2018. https://doi.org/10.1029/2006GB002840

Borbon, A., Gilman, J. B., Kuster, W. C., Grand, N., Chevaillier, S., Colomb, A., et al. (2013). Emission ratios of anthropogenic volatile organic compounds in northern mid-latitude megacities: Observations versus emission inventories in Los Angeles and Paris. *Journal of Geophysical Research: Atmospheres*, *118*, 2041–2057. https://doi.org/10.1002/jgrd.50059

Bressi, M., Cavalli, F., Belis, C. A., Putaud, J. P., Fröhlich, R., Martins dos Santos, S., et al. (2016). Variations in the chemical composition of the submicron aerosol and in the sources of the organic fraction at a regional background site of the Po Valley (Italy). *Atmospheric Chemistry and Physics*, *16*(20), 12,875–12,896. https://doi.org/10.5194/acp-16-12875-2016

Brock, C. A., Wagner, N. L., Anderson, B. E., Attwood, A. R., Beyersdorf, A., Campuzano-Jost, P., et al. (2016). Aerosol optical properties in the southeastern United States in summer—Part 1: Hygroscopic growth. *Atmospheric Chemistry and Physics*, *16*(8), 4987–5007. https://doi.org/10.5194/acp-16-4987-2016

Budisulistiorini, S. H., Baumann, K., Edgerton, E. S., Bairai, S. T., Mueller, S., Shaw, S. L., et al. (2016). Seasonal characterization of submicron aerosol chemical composition and organic aerosol sources in the southeastern United States: Atlanta, Georgia,and Look Rock, Tennessee. *Atmospheric Chemistry and Physics*, *16*(8), 5171–5189. https://doi.org/10.5194/acp-16-5171-2016

Cai, Y., Montague, D. C., Mooiweer-Bryan, W., & Deshler, T. (2008). Performance characteristics of the ultra high sensitivity aerosol spectrometer for particles between 55 and 800 nm: Laboratory and field studies. *Journal of Aerosol Science*, *39*(9), 759–769. https://doi.org/10.1016/j.jaerosci.2008.04.007

Calvert, J. G., Orlando, J. J., Stockwell, W. R., & Wallington, T. J. (2015). *The mechanisms of reactions influencing atmospheric ozone*. New York: Oxford University Press.

Canagaratna, M. R., Jayne, J. T., Jimenez, J. L., Allan, J. D., Alfarra, M. R., Zhang, Q., et al. (2007). Chemical and microphysical characterization of ambient aerosols with the aerodyne aerosol mass spectrometer. *Mass Spectrometry Reviews*, *26*(2), 185–222. https://doi.org/10.1002/mas

Canagaratna, M. R., Jimenez, J. L., Kroll, J. H., Chen, Q., Kessler, S. H., Massoli, P., et al. (2015). Elemental ratio measurements of organic compounds using aerosol mass spectrometry: characterization, improved calibration, and implications. *Atmospheric Chemistry and Physics*, *15*(1), 253–272. https://doi.org/10.5194/acp-15-253-2015

Cao, J. J., Lee, S. C., Ho, K. F., Zhang, X. Y., Zou, S. C., Fung, K., et al. (2003). Characteristics of carbonaceous aerosol in Pearl River Delta Region, China during 2001 winter period. *Atmospheric Environment*, *37*(11), 1451–1460. https://doi.org/10.1016/S1352-2310(02)01002-6

Castro, L. M., Pio, C. A., Harrison, R. M., & Smith, D. J. T. (1999). Carbonaceous aerosol in urban and rural European atmospheres: Estimation of secondary organic carbon concentrations. *Atmospheric Environment*, *33*(17), 2771–2781. https://doi.org/10.1016/S1352-2310(98)00331-8

Cevik, B. K., Rutter, A. P., Gong, L., Griffin, R. J., Flynn, J. H., Lefer, B. L., & Kim, S. (2016). Airmass aging metrics derived from particle and other measurements near Fort Worth. *Atmospheric Environment*, *126*, 45–54. https://doi.org/10.1016/j.atmosenv.2015.11.044

Chen, Q., Heald, C. L., Jimenez, J. L., Canagaratna, M. R., Zhang, Q., He, L. Y., et al. (2015). Elemental composition of organic aerosol: The gap between ambient and laboratory measurements. *Geophysical Research Letters*, *42*, 4182–4189. https://doi.org/10.1002/2015GL063693

Crippa, M., DeCarlo, P. F., Slowik, J. G., Mohr, C., Heringa, M. F., Chirico, R., et al. (2013). Wintertime aerosol chemical composition and source apportionment of the organic fraction in the metropolitan area of Paris. *Atmospheric Chemistry and Physics*, *13*(2), 961–981. https://doi.org/10.5194/acp-13-961-2013

Crounse, J. D., DeCarlo, P. F., Blake, D. R., Emmons, L. K., Campos, T. L., Apel, E. C., et al. (2009). Biomass burning and urban air pollution over the Central Mexican Plateau. *Atmospheric Chemistry and Physics Discussions*, *9*(1), 2699–2734. https://doi.org/10.5194/acpd-9-2699-2009

Crounse, J. D., Nielsen, L. B., Jørgensen, S., Kjaergaard, H. G., & Wennberg, P. O. (2013). Autoxidation of organic compounds in the atmosphere. *Journal of Physical Chemistry Letters*, *4*(20), 3513–3520. https://doi.org/10.1021/jz4019207

Cubison, M. J., Ortega, A. M., Hayes, P. L., Farmer, D. K., Day, D., Lechner, M. J., et al. (2011). Effects of aging on organic aerosol from open biomass burning smoke in aircraft and laboratory studies. *Atmospheric Chemistry and Physics*, *11*(23), 12,049–12,064. https://doi.org/10.5194/acp-11-12049-2011

Day, D. A., Liu, S., Russell, L. M., & Ziemann, P. J. (2010). Organonitrate group concentrations in submicron particles with high nitrate and organic fractions in coastal southern California. *Atmospheric Environment*, *44*(16), 1970–1979. https://doi.org/10.1016/j.atmosenv.2010.02.045

DeCarlo, P. F., Dunlea, E. J., Kimmel, J. R., Aiken, A. C., Sueper, D., Crounse, J., et al. (2008). Fast airborne aerosol size and chemistry measurements above Mexico City and Central Mexico during the MILAGRO campaign. *Atmospheric Chemistry and Physics*, *8*(14), 4027–4048. https://doi.org/10.5194/acp-8-4027-2008

DeCarlo, P. F., Slowik, J. G., Worsnop, D. R., Davidovits, P., & Jimenez, J. L. (2004). Particle morphology and density characterization by combined mobility and aerodynamic diameter measurements. Part 1: Theory. *Aerosol Science and Technology*, *38*(12), 1185–1205. https://doi.org/10.1080/027868290903907

DeCarlo, P. F., Ulbrich, I. M., Crounse, J., de Foy, B., Dunlea, E. J., Aiken, A. C., et al. (2010). Investigation of the sources and processing of organic aerosol over the Central Mexican Plateau from aircraft measurements during MILAGRO. *Atmospheric Chemistry and Physics*, *10*(12), 5257–5280. https://doi.org/10.5194/acp-10-5257-2010

DeCarlo, P. F., Kimmel, J. R., Trimborn, A., Northway, M. J., Jayne, J. T., Aiken, A. C., et al. (2006). Field-deployable, high-resolution, time-of-flight aerosol mass spectrometer. *Analytical Chemistry*, *78*(24), 8281–8289. https://doi.org/10.1021/ac061249n

Dibb, J. E. (2003). Aerosol chemical composition in Asian continental outflow during the TRACE-P campaign: Comparison with PEM-West B. *Journal of Geophysical Research*, *108*(D21), 8815. https://doi.org/10.1029/2002JD003111

Dibb, J. E., Talbot, R. W., Seid, G., Jordan, C., Scheuer, E., Atlas, E., et al. (2002). Airborne sampling of aerosol particles: Comparison between surface sampling at Christmas Island and P-3 sampling during PEM-Tropics B. *Journal of Geophysical Research*, *108*(D2), 8230. https://doi.org/10.1029/2001JD000408

Ding, X., He, Q.-F., Shen, R.-Q., Yu, Q.-Q., Zhang, Y.-Q., Xin, J.-Y., et al. (2016). Spatial and seasonal variations of isoprene secondary organic aerosol in China: Significant impact of biomass burning during winter. *Scientific Reports*, *6*(1), 20411. https://doi.org/10.1038/srep20411

Ding, X., Zhang, Y., He, Q., Yu, Q., Wang, J.-Q., Shen, R., et al. (2017). Significant increase of aromatics-derived secondary organic aerosol during fall to winter in China. *Environmental Science & Technology*, *51*(13), 7432–7441. https://doi.org/10.1021/acs.est.6b06408

Docherty, K. S., Aiken, A. C., Huffman, J. A., Ulbrich, I. M., DeCarlo, P. F., Sueper, D., et al. (2011). The 2005 Study of Organic Aerosols at Riverside (SOAR-1): Instrumental intercomparisons and fine particle composition. *Atmospheric Chemistry and Physics*, *11*(23), 12,387–12,420. https://doi.org/10.5194/acp-11-12387-2011

Docherty, K. S., Stone, E. A., Ulbrich, I. M., DeCarlo, P. F., Snyder, D. C., Schauer, J. J., et al. (2008). Apportionment of primary and secondary organic aerosols in Southern California during the 2005 Study of Organic Aerosols in Riverside (SOAR-1). *Environmental Science & Technology*, *42*(20), 7655–7662. https://doi.org/10.1021/Es8008166

Donahue, N. M., Epstein, S. A., Pandis, S. N., & Robinson, A. L. (2011). A two-dimensional volatility basis set: 1. Organic-aerosol mixing thermodynamics. *Atmospheric Chemistry and Physics*, *11*(7), 3303–3318. https://doi.org/10.5194/acp-11-3303-2011

Donahue, N. M., Robinson, A. L., Stanier, C. O., & Pandis, S. N. (2006). Coupled partitioning, dilution, and chemical aging of semivolatile organics. *Environmental Science & Technology*, *40*(8), 2635–2643. https://doi.org/10.1021/es052297c

Drewnick, F., Schwab, J. J., Jayne, J. T., Canagaratna, M., Worsnop, D. R., & Demerjian, K. L. (2004). Measurement of ambient aerosol composition during the PMTACS-NY 2001 using an aerosol mass spectrometer. Part I: Mass concentrations special issue of aerosol science and technology on findings from the fine particulate matter supersites program. *Aerosol Science and Technology*, *38*(S1), 92–103. https://doi.org/10.1080/02786820390229507

Dunlea, E. J., DeCarlo, P. F., Aiken, A. C., Kimmel, J. R., Peltier, R. E., Weber, R. J., et al. (2009). Evolution of Asian aerosols during transpacific transport in INTEX-B. *Atmospheric Chemistry and Physics*, *9*(19), 7257–7287. https://doi.org/10.5194/acp-9-7257-2009

EDGAR (2018). EDGAR v4.2 global emissions. Retrieved from http://edgar.jrc.ec.europa.eu/overview.php?v=42, (Accessed 2 February 2018).

Ehn, M., Thornton, J. A., Kleist, E., Sipilä, M., Junninen, H., Pullinen, I., et al. (2014). A large source of low-volatility secondary organic aerosol. *Nature*, *506*(7489), 476–479. https://doi.org/10.1038/nature13032

Emmerson, K. M., Carslaw, N., & Pilling, M. J. (2005). Urban atmospheric chemistry during the PUMA campaign 2: Radical budgets for OH, HO_2 and RO_2. *Journal of Atmospheric Chemistry*, *52*(2), 165–183. https://doi.org/10.1007/s10874-005-1323-2

Environmental Protection Agency (2015). Standards of performance for new residential wood heaters, new residential hydronic heaters and forced-air furnaces. Final Rule, 80 Fed. Regist. 50 (March 16, 2015), 13671–13753.

Ervens, B. (2015). Modeling the processing of aerosol and trace gases in clouds and fogs. *Chemical Reviews*, *115*(10), 4157–4198. https://doi.org/10.1021/cr5005887

Farmer, D. K., Matsunaga, A., Docherty, K. S., Surratt, J. D., Seinfeld, J. H., Ziemann, P. J., & Jimenez, J. L. (2010). Response of an aerosol mass spectrometer to organonitrates and organosulfates and implications for atmospheric chemistry. *Proceedings of the National Academy of Sciences of the United States of America*, *107*(15), 6670–6675. https://doi.org/10.1073/pnas.0912340107

Fibiger, D. L., McDuffie, E. E., Dubé, W. P., Aikin, K. C., Lopez-Hilfiker, F. D., Lee, B. H., et al. (2018). Wintertime overnight NO_x removal in a southeastern United States coal-fired power plant plume: A model for understanding winter NO_x processing and its implications. *Journal of Geophysical Research: Atmospheres*, *123*, 1412–1425. https://doi.org/10.1002/2017JD027768

Freney, E. J., Sellegri, K., Canonaco, F., Colomb, A., Borbon, A., Michoud, V., et al. (2014). Characterizing the impact of urban emissions on regional aerosol particles: airborne measurements during the MEGAPOLI experiment. *Atmospheric Chemistry and Physics*, *14*(3), 1397–1412. https://doi.org/10.5194/acp-14-1397-2014

Fry, J. L., Draper, D. C., Zarzana, K. J., Campuzano-Jost, P., Day, D. A., Jimenez, J. L., et al. (2013). Observations of gas- and aerosol-phase organic nitrates at BEACHON-RoMBAS 2011. *Atmospheric Chemistry and Physics*, *13*(17), 8585–8605. https://doi.org/10.5194/acp-13-8585-2013

Ge, X., Setyan, A., Sun, Y., & Zhang, Q. (2012). Primary and secondary organic aerosols in Fresno, California during wintertime: Results from high resolution aerosol mass spectrometry. *Journal of Geophysical Research*, *117*, D19301. https://doi.org/10.1029/2012JD018026

GEOS-Chem (2017). GEOS-Chem wiki. Retrieved from http://wiki.seas.harvard.edu/geos-chem/index.php/Main_Page, (Accessed 27 December 2017).

Gilardoni, S., Massoli, P., Paglione, M., Giulianelli, L., Carbone, C., Rinaldi, M., et al. (2016). Direct observation of aqueous secondary organic aerosol from biomass-burning emissions. *Proceedings of the National Academy of Sciences of the United States of America*, *113*(36), 10,013–10,018. https://doi.org/10.1073/pnas.1602212113

Gligorovski, S., Strekowski, R., Barbati, S., & Vione, D. (2015). Environmental implications of hydroxyl radicals (˙OH). *Chemical Reviews*, *115*(24), 13,051–13,092. https://doi.org/10.1021/cr500310b

de Gouw, J. A., Brock, C. A., Atlas, E. L., Bates, T. S., Fehsenfeld, F. C., Goldan, P. D., et al. (2008). Sources of particulate matter in the northeastern United States in summer: 1. Direct emissions and secondary formation of organic matter in urban plumes. *Journal of Geophysical Research*, *113*, D08301. https://doi.org/10.1029/2007JD009243

de Gouw, J. A., Middlebrook, A. M., Warneke, C., Goldan, P. D., Kuster, W. C., Roberts, J. M., et al. (2005). Budget of organic carbon in a polluted atmosphere: Results from the New England Air Quality Study in 2002. *Journal of Geophysical Research*, *110*, D16305. https://doi.org/10.1029/2004JD005623

Griffin, R. J., Chen, J., Carmody, K., Vutukuru, S., & Dabdub, D. (2007). Contribution of gas phase oxidation of volatile organic compounds to atmospheric carbon monoxide levels in two areas of the United States. *Journal of Geophysical Research*, *112*, D10S17. https://doi.org/10.1029/2006JD007602

Guenther, A. B., Jiang, X., Heald, C. L., Sakulyanontvittaya, T., Duhl, T., Emmons, L. K., & Wang, X. (2012). The model of emissions of gases and aerosols from nature version 2.1 (MEGAN2.1): An extended and updated framework for modeling biogenic emissions. *Geoscientific Model Development*, *5*(6), 1471–1492. https://doi.org/10.5194/gmd-5-1471-2012

Guo, H., Sullivan, A. P., Campuzano-Jost, P., Schroder, J. C., Lopez-Hilfiker, F. D., Dibb, J. E., et al. (2016). Fine particle pH and the partitioning of nitric acid during winter in the northeastern United States. *Journal of Geophysical Research: Atmospheres*, *121*, 10,355–10,376. https://doi.org/10.1002/2016JD025311

Hand, J. L., & Kreidenweis, S. M. (2002). A new method for retrieving particle refractive index and effective density from aerosol size distribution data. *Aerosol Science and Technology*, *36*(10), 1012–1026. https://doi.org/10.1080/02786820290092276

Hand, J. L., Schichtel, B. A., Pitchford, M., Malm, W. C., & Frank, N. H. (2012). Seasonal composition of remote and urban fine particulate matter in the United States. *Journal of Geophysical Research*, *117*, D05209. https://doi.org/10.1029/2011JD017122

Hayes, P. L., Carlton, A. G., Baker, K. R., Ahmadov, R., Washenfelder, R. A., Alvarez, S., et al. (2015). Modeling the formation and aging of secondary organic aerosols in Los Angeles during CalNex 2010. *Atmospheric Chemistry and Physics*, *15*(10), 5773–5801. https://doi.org/10.5194/acp-15-5773-2015

Hayes, P. L., Ortega, A. M., Cubison, M. J., Froyd, K. D., Zhao, Y., Cliff, S. S., et al. (2013). Organic aerosol composition and sources in Pasadena, California, during the 2010 CalNex campaign. *Journal of Geophysical Research: Atmospheres*, *118*, 9233–9257. https://doi.org/10.1002/jgrd.50530

Heald, C. L., Kroll, J. H., Jimenez, J. L., Docherty, K. S., DeCarlo, P. F., Aiken, A. C., et al. (2010). A simplified description of the evolution of organic aerosol composition in the atmosphere. *Geophysical Research Letters*, *37*, L08803. https://doi.org/10.1029/2010GL042737

Heard, D. E., Carpenter, L. J., Creasey, D. J., Hopkins, J. R., Lee, J. D., Lewis, A. C., et al. (2004). High levels of the hydroxyl radical in the winter urban troposphere. *Geophysical Research Letters*, *31*, L18112. https://doi.org/10.1029/2004GL020544

Hennigan, C. J., Sandholm, S., Kim, S., Stickel, R. E., Huey, L. G., & Weber, R. J. (2006). Influence of Ohio River valley emissions on fine particle sulfate measured from aircraft over large regions of the eastern United States and Canada during INTEX-NA. *Journal of Geophysical Research*, *111*, D24S04. https://doi.org/10.1029/2006JD007282

Henze, D. K., Seinfeld, J. H., Ng, N. L., Kroll, J. H., Fu, T.-M., Jacob, D. J., & Heald, C. L. (2008). Global modeling of secondary organic aerosol formation from aromatic hydrocarbons: High- vs. low-yield pathways. *Atmospheric Chemistry and Physics*, *8*(9), 2405–2420. https://doi.org/10.5194/acp-8-2405-2008

HIMIL (2018). HIAPER modular inlet. Retrieved from https://www.eol.ucar.edu/instruments/hiaper-modular-inlet, (Accessed 16 January 2018).

Hodzic, A., & Jimenez, J. L. (2011). Modeling anthropogenically controlled secondary organic aerosols in a megacity: A simplified framework for global and climate models. *Geoscientific Model Development*, *4*(4), 901–917. https://doi.org/10.5194/gmd-4-901-2011

Hodzic, A., Kasibhatla, P. S., Jo, D. S., Cappa, C. D., Jimenez, J. L., Madronich, S., & Park, R. J. (2016). Rethinking the global secondary organic aerosol (SOA) budget: Stronger production, faster removal, shorter lifetime. *Atmospheric Chemistry and Physics*, *16*(12), 7917–7941. https://doi.org/10.5194/acp-16-7917-2016

Hornbrook, R. S., Blake, D. R., Diskin, G. S., Fried, A., Fuelberg, H. E., Meinardi, S., et al. (2011). Observations of nonmethane organic compounds during ARCTAS—Part 1: Biomass burning emissions and plume enhancements. *Atmospheric Chemistry and Physics*, *11*(21), 11,103–11,130. https://doi.org/10.5194/acp-11-11103-2011

Hu, W., Campuzano-Jost, P., Day, D. A., Croteau, P., Canagaratna, M. R., Jayne, J. T., et al. (2017). Evaluation of the new capture vaporizer for aerosol mass spectrometers (AMS) through field studies of inorganic species. *Aerosol Science and Technology*, *51*(6), 735–754. https://doi.org/10.1080/02786826.2017.1296104

Hu, W., Hu, M., Hu, W., Jimenez, J. L., Yuan, B., Chen, W., et al. (2016). Chemical composition, sources, and aging process of submicron aerosols in Beijing: Contrast between summer and winter. *Journal of Geophysical Research: Atmospheres*, *121*, 1955–1977. https://doi.org/10.1002/2015JD024020

Hu, W. W., Campuzano-Jost, P., Palm, B. B., Day, D. A., Ortega, A. M., Hayes, P. L., et al. (2015). Characterization of a real-time tracer for isoprene epoxydiols-derived secondary organic aerosol (IEPOX-SOA) from aerosol mass spectrometer measurements. *Atmospheric Chemistry and Physics*, *15*(20), 11,807–11,833. https://doi.org/10.5194/acp-15-11807-2015

Huang, X. F., Xue, L., Tian, X. D., Shao, W. W., Le Sun, T., Gong, Z. H., et al. (2013). Highly time-resolved carbonaceous aerosol characterization in Yangtze River Delta of China: Composition, mixing state and secondary formation. *Atmospheric Environment*, *64*, 200–207. https://doi.org/10.1016/j.atmosenv.2012.09.059

Jaeglé, L., Shah, V., Thornton, J. A., Lopez-Hilfiker, F. D., & Lee, B. (2017). Wintertime emissions and chemistry over the N.E. US: Role of oxidants and heterogeneous chemistry. In *The 8th International GEOS-Chem Meeting*. Cambridge, MA.

Jayne, J. T., Leard, D. C., Zhang, X. F., Davidovits, P., Smith, K. A., Kolb, C. E., & Worsnop, D. R. (2000). Development of an aerosol mass spectrometer for size and composition analysis of submicron particles. *Aerosol Science and Technology*, *33*(1–2), 49–70.

Jimenez, J. L., Canagaratna, M. R., Donahue, N. M., Prevot, A. S. H., Zhang, Q., Kroll, J. H., et al. (2009). Evolution of organic aerosols in the atmosphere. *Science*, *326*(5959), 1525–1529. https://doi.org/10.1126/science.1180353

Jo, D. S., Park, R. J., Kim, M. J., & Spracklen, D. V. (2013). Effects of chemical aging on global secondary organic aerosol using the volatility basis set approach. *Atmospheric Environment*, *81*, 230–244. https://doi.org/10.1016/j.atmosenv.2013.08.055

Jolleys, M. D., Coe, H., McFiggans, G., Capes, G., Allan, J. D., Crosier, J., et al. (2012). Characterizing the aging of biomass burning organic aerosol by use of mixing ratios: A meta-analysis of four regions. *Environmental Science & Technology*, *46*(24), 13,093–13,102. https://doi.org/10.1021/es302386v

Kiendler-Scharr, A., Mensah, A. A., Friese, E., Topping, D., Nemitz, E., Prevot, A. S. H., et al. (2016). Ubiquity of organic nitrates from nighttime chemistry in the European submicron aerosol. *Geophysical Research Letters*, *43*, 7735–7744. https://doi.org/10.1002/2016GL069239

Kim, H., Zhang, Q., Gwi-Nam, B., Young Kim, J., & Bok Lee, S. (2017). Sources and atmospheric processing of winter aerosols in Seoul, Korea: Insights from real-time measurements using a high-resolution aerosol mass spectrometer. *Atmospheric Chemistry and Physics*, *17*(3), 2009–2033. https://doi.org/10.5194/acp-17-2009-2017

Kim, P. S., Jacob, D. J., Fisher, J. A., Travis, K., Yu, K., Zhu, L., et al. (2015). Sources, seasonality, and trends of Southeast US aerosol: An integrated analysis of surface, aircraft, and satellite observations with the GEOS-Chem chemical transport model. *Atmospheric Chemistry and Physics*, *15*(18), 10,411–10,433. https://doi.org/10.5194/acp-15-10411-2015

Kimmel, J. R., Farmer, D. K., Cubison, M. J., Sueper, D., Tanner, C., Nemitz, E., et al. (2011). Real-time aerosol mass spectrometry with millisecond resolution. *International Journal of Mass Spectrometry*, *303*(1), 15–26. https://doi.org/10.1016/j.ijms.2010.12.004

Kleinman, L. I., Daum, P. H., Lee, Y. N., Nunnermacker, L. J., Springston, S. R., Weinstein-Lloyd, J., et al. (2003). Photochemical age determinations in the Phoenix metropolitan area. *Journal of Geophysical Research*, *108*(D3), 4096. https://doi.org/10.1029/2002JD002621

Kleinman, L. I., Daum, P. H., Lee, Y. N., Senum, G. I., Springston, S. R., Wang, J., et al. (2007). Aircraft observations of aerosol composition and ageing in New England and Mid-Atlantic States during the summer 2002 New England Air Quality Study field campaign. *Journal of Geophysical Research*, *112*, D09310. https://doi.org/10.1029/2006JD007786

Kleinman, L. I., Springston, S. R., Daum, P. H., Lee, Y. N., Nunnermacker, L. J., Senum, G. I., et al. (2008). The time evolution of aerosol composition over the Mexico City plateau. *Atmospheric Chemistry and Physics*, *8*(6), 1559–1575. https://doi.org/10.5194/acp-8-1559-2008

Knote, C., Brunner, D., Vogel, H., Allan, J., Asmi, A., Äijälä, M., et al. (2011). Towards an online-coupled chemistry-climate model: Evaluation of trace gases and aerosols in COSMO-ART. *Geoscientific Model Development*, *4*(4), 1077–1102. https://doi.org/10.5194/gmd-4-1077-2011

Koo, B., Knipping, E., & Yarwood, G. (2014). 1.5-Dimensional volatility basis set approach for modeling organic aerosol in CAMx and CMAQ. *Atmospheric Environment*, *95*, 158–164. https://doi.org/10.1016/j.atmosenv.2014.06.031

Kupc, A., Williamson, C., Wagner, N. L., Richardson, M., & Brock, C. A. (2017). Modification, calibration, and performance of the Ultra-High Sensitivity Aerosol Spectrometer for particle size distribution and volatility measurements during the Atmospheric Tomography (ATom) airborne campaign. *Atmospheric Measurement Techniques Discussions*, 1–25. https://doi.org/10.5194/amt-2017-293

Kuwata, M., Zorn, S. R., & Martin, S. T. (2012). Using elemental ratios to predict the density of organic material composed of carbon, hydrogen, and oxygen. *Environmental Science & Technology*, *46*(2), 787–794. https://doi.org/10.1021/es202525q

Lanz, V. A., Alfarra, M. R., Baltensperger, U., Buchmann, B., Hueglin, C., Szidat, S., et al. (2008). Source attribution of submicron organic aerosols during wintertime inversions by advanced factor analysis of aerosol mass spectra. *Environmental Science & Technology*, *42*(1), 214–220. https://doi.org/10.1021/es0707207

Local Climatological Data (2018), NOAA: National Centers for Environmental Information—Data tools: Local Climatological Data (LCD). Available at https://www.ncdc.noaa.gov/cdo-web/datatools/lcd (Accessed 2 February 2018)

Lee, C., Martin, R. V., van Donkelaar, A., Lee, H., Dickerson, R. R., Hains, J. C., et al. (2011). SO_2 emissions and lifetimes: Estimates from inverse modeling using in situ and global, space-based (SCIAMACHY and OMI) observations. *Journal of Geophysical Research*, *116*, D06304. https://doi.org/10.1029/2010JD014758

Liao, J., Froyd, K. D., Murphy, D. M., Keutsch, F. N., Yu, G., Wennberg, P. O., et al. (2015). Airborne measurements of organosulfates over the continental U.S. *Journal of Geophysical Research: Atmospheres*, *120*, 2990–3005. https://doi.org/10.1002/2014JD022378

Liu, P. S. K., Leaitch, W. R., Strapp, J. W., & Wasey, M. A. (1992). Response of particle measuring systems airborne ASASP and PCASP to NaCl and latex particles. *Aerosol Science and Technology*, *16*(2), 83–95. https://doi.org/10.1080/02786829208959539

Liu, X., Huey, L. G., Yokelson, R. J., Selimovic, V., Simpson, I. J., Müller, M., et al. (2017). Airborne measurements of western U.S. wildfire emissions: Comparison with prescribed burning and air quality implications. *Journal of Geophysical Research: Atmospheres*, *122*, 6108–6129. https://doi.org/10.1002/2016JD026315

Liu, X., Zhang, Y., Huey, L. G., Yokelson, R. J., Wang, Y., Jimenez, J. L., et al. (2016). Agricultural fires in the southeastern U.S. during SEAC 4 RS: Emissions of trace gases and particles and evolution of ozone, reactive nitrogen, and organic aerosol. *Journal of Geophysical Research: Atmospheres*, *121*, 7383–7414. https://doi.org/10.1002/2016JD025040

Louvaris, E. E., Florou, K., Karnezi, E., Papanastasiou, D. K., Gkatzelis, G. I., & Pandis, S. N. (2017). Volatility of source apportioned wintertime organic aerosol in the city of Athens. *Atmospheric Environment*, *158*, 138–147. https://doi.org/10.1016/j.atmosenv.2017.03.042

Ma, P. K., Zhao, Y., Robinson, A. L., Worton, D. R., Goldstein, A. H., Ortega, A. M., et al. (2017). Evaluating the impact of new observational constraints on P-S/IVOC emissions, multi-generation oxidation, and chamber wall losses on SOA modeling for Los Angeles, CA. *Atmospheric Chemistry and Physics*, *17*(15), 9237–9259. https://doi.org/10.5194/acp-17-9237-2017

Mao, J., Ren, X., Brune, W. H., Olson, J. R., Crawford, J. H., Fried, A., et al. (2009). Airborne measurement of OH reactivity during INTEX-B. *Atmospheric Chemistry and Physics*, *9*(1), 163–173. https://doi.org/10.5194/acp-9-163-2009

Marais, E. A., Jacob, D. J., Jimenez, J. L., Campuzano-Jost, P., Day, D. A., Hu, W., et al. (2016). Aqueous-phase mechanism for secondary organic aerosol formation from isoprene: Application to the southeast United States and co-benefit of SO_2 emission controls. *Atmospheric Chemistry and Physics*, *16*(3), 1603–1618. https://doi.org/10.5194/acp-16-1603-2016

McDonald, B. C., de Gouw, J. A., Gilman, J. B., Jathar, S. H., Akherati, A., Cappa, C. D., et al. (2018). Volatile chemical products emerging as largest petrochemical source of urban organic emissions. *Science*, *359*(6377), 760–764. https://doi.org/10.1126/science.aaq0524

McMeeking, G. R., Bart, M., Chazette, P., Haywood, J. M., Hopkins, J. R., McQuaid, J. B., et al. (2012). Airborne measurements of trace gases and aerosols over the London metropolitan region. *Atmospheric Chemistry and Physics*, *12*(11), 5163–5187. https://doi.org/10.5194/acp-12-5163-2012

McNaughton, C. S., Clarke, A. D., Howell, S. G., Pinkerton, M., Anderson, B., Thornhill, L., et al. (2007). Results from the DC-8 Inlet Characterization Experiment (DICE): Airborne versus surface sampling of mineral dust and sea salt aerosols. *Aerosol Science and Technology*, *41*(2), 136–159. https://doi.org/10.1080/02786820601118406

Middlebrook, A. M., Bahreini, R., Jimenez, J. L., & Canagaratna, M. R. (2012). Evaluation of composition-dependent collection efficiencies for the Aerodyne Aerosol Mass Spectrometer using field data. *Aerosol Science and Technology*, *46*(3), 258–271. https://doi.org/10.1080/02786826.2011.620041

Moharreri, A., Craig, L., Dubey, P., Rogers, D. C., & Dhaniyala, S. (2014). Aircraft testing of the new Blunt-body Aerosol Sampler (BASE). *Atmospheric Measurement Techniques*, *7*(9), 3085–3093. https://doi.org/10.5194/amt-7-3085-2014

Mohr, C., DeCarlo, P. F., Heringa, M. F., Chirico, R., Slowik, J. G., Richter, R., et al. (2012). Identification and quantification of organic aerosol from cooking and other sources in Barcelona using aerosol mass spectrometer data. *Atmospheric Chemistry and Physics*, *12*(4), 1649–1665. https://doi.org/10.5194/acp-12-1649-2012

Murphy, B. N., Woody, M. C., Jimenez, J. L., Carlton, A. M. G., Hayes, P. L., Liu, S., et al. (2017). Semivolatile POA and parameterized total combustion SOA in CMAQv5.2: Impacts on source strength and partitioning. *Atmospheric Chemistry and Physics*, *17*(18), 11,107–11,133. https://doi.org/10.5194/acp-17-11107-2017

Myhre, G., Shindell, D., Bréon, F.-M., Collins, W., Fuglestvedt, J., Huang, J., et al. (2013). Anthropogenic and natural radiative forcing. In T. F. Stocker, D. Qin, G.-K. Plattner, M. Tignor, S. K. Allen, J. Boschung, et al. (Eds.), *Climate change 2013: The physical science basis* (pp. 659–740). Cambridge, UK and New York: Cambridge University Press.

NEI (2018). U.S. EPA 2011 version 6 emissions modeling platform based on the National Emissions Inventory (NEI) 2011 v1. Retrieved from https://www.epa.gov/air-emissions-modeling/2011-version-6-air-emissions-modeling-platforms, (Accessed 1 January 2018).

Ng, N. L., Brown, S. S., Archibald, A. T., Atlas, E., Cohen, R. C., Crowley, J. N., et al. (2017). Nitrate radicals and biogenic volatile organic compounds: Oxidation, mechanisms, and organic aerosol. *Atmospheric Chemistry and Physics*, *17*(3), 2103–2162. https://doi.org/10.5194/acp-17-2103-2017

Ng, N. L., Canagaratna, M. R., Jimenez, J. L., Chhabra, P. S., Seinfeld, J. H., & Worsnop, D. R. (2011). Changes in organic aerosol composition with aging inferred from aerosol mass spectra. *Atmospheric Chemistry and Physics*, *11*(13), 6465–6474. https://doi.org/10.5194/acp-11-6465-2011

Ng, N. L., Canagaratna, M. R., Zhang, Q., Jimenez, J. L., Tian, J., Ulbrich, I. M., et al. (2010). Organic aerosol components observed in Northern Hemispheric datasets from Aerosol Mass Spectrometry. *Atmospheric Chemistry and Physics*, *10*(10), 4625–4641. https://doi.org/10.5194/acp-10-4625-2010

Odum, J. R., Jungkamp, T. P. W., Griffin, R. J., Flagan, R. C., & Seinfeld, J. H. (1997). The atmospheric aerosol-forming potential of whole gasoline vapor. *Science*, *276*(5309), 96–99. https://doi.org/10.1126/science.276.5309.96

Olszyna, K. J., Bailey, E. M., Simonaitis, R., & Meagher, J. F. (1994). O_3 and NO_y relationships at a rural site. *Journal of Geophysical Research*, *99*(D7), 14,557–14,563. https://doi.org/10.1029/94JD00739

Orsini, D. A., Ma, Y., Sullivan, A., Sierau, B., Baumann, K., & Weber, R. J. (2003). Refinements to the particle-into-liquid sampler (PILS) for ground and airborne measurements of water soluble aerosol composition. *Atmospheric Environment*, *37*(9–10), 1243–1259. https://doi.org/10.1016/S1352-2310(02)01015-4

Ortega, A. M., Hayes, P. L., Peng, Z., Palm, B. B., Hu, W., Day, D. A., et al. (2016). Real-time measurements of secondary organic aerosol formation and aging from ambient air in an oxidation flow reactor in the Los Angeles area. *Atmospheric Chemistry and Physics*, *16*(11), 7411–7433. https://doi.org/10.5194/acp-16-7411-2016

Öztürk, F., Bahreini, R., Wagner, N. L., Dubé, W. P., Young, C. J., Brown, S. S., et al. (2013). Vertically resolved chemical characteristics and sources of submicron aerosols measured on a Tall Tower in a suburban area near Denver, Colorado in winter. *Journal of Geophysical Research: Atmospheres*, *118*, 13,591–13,605. https://doi.org/10.1002/2013JD019923

Palm, B. B., Campuzano-Jost, P., Ortega, A. M., Day, D. A., Kaser, L., Jud, W., et al. (2016). In situ secondary organic aerosol formation from ambient pine forest air using an oxidation flow reactor. *Atmospheric Chemistry and Physics*, *16*(5), 2943–2970. https://doi.org/10.5194/acp-16-2943-2016

Park, R. J. (2003). Sources of carbonaceous aerosols over the United States and implications for natural visibility. *Journal of Geophysical Research*, *108*(D12), 4355. https://doi.org/10.1029/2002JD003190

Park, R. J., Jacob, D. J., Field, B. D., Yantosca, R. M., & Chin, M. (2004). Natural and transboundary pollution influences on sulfate-nitrate-ammonium aerosols in the United States: Implications for policy. *Journal of Geophysical Research*, *109*, D15204. https://doi.org/10.1029/2003JD004473

Parrella, J. P., Jacob, D. J., Liang, Q., Zhang, Y., Mickley, L. J., Miller, B., et al. (2012). Tropospheric bromine chemistry: Implications for present and pre-industrial ozone and mercury. *Atmospheric Chemistry and Physics*, *12*(15), 6723–6740. https://doi.org/10.5194/acp-12-6723-2012

Parrish, D. D., Stohl, A., Forster, C., Atlas, E. L., Blake, D. R., Goldan, P. D., et al. (2007). Effects of mixing on evolution of hydrocarbon ratios in the troposphere. *Journal of Geophysical Research*, *112*, D10S34. https://doi.org/10.1029/2006JD007583

Peltier, R. E., Sullivan, A. P., Weber, R. J., Brock, C. A., Wollny, A. G., Holloway, J. S., et al. (2007). Fine aerosol bulk composition measured on WP-3D research aircraft in vicinity of the Northeastern United States—Results from NEAQS. *Atmospheric Chemistry and Physics*, *7*(12), 3231–3247. https://doi.org/10.5194/acp-7-3231-2007

Pieber, S. M., el Haddad, I., Slowik, J. G., Canagaratna, M. R., Jayne, J. T., Platt, S. M., et al. (2016). Inorganic salt interference on CO_2^+ in aerodyne AMS and ACSM organic aerosol composition studies. *Environmental Science & Technology*, *50*(19), 10,494–10,503. https://doi.org/10.1021/acs.est.6b01035

Pirjola, L., Niemi, J. V., Saarikoski, S., Aurela, M., Enroth, J., Carbone, S., et al. (2017). Physical and chemical characterization of urban wintertime aerosols by mobile measurements in Helsinki, Finland. *Atmospheric Environment*, *158*, 60–75. https://doi.org/10.1016/j.atmosenv.2017.03.028

Pope, C. A. III, Burnett, R. T., Thun, M. J., Calle, E. E., Krewski, D., Ito, K., & Thursten, G. D. (2002). Lung cancer, cardiopulmonary mortality, and long-term exposure to fine particulate air pollution. *Journal of the American Medical Association*, *287*(9), 1132–1141. https://doi.org/10.1001/jama.287.9.1132

Poulain, L., Spindler, G., Birmili, W., Plass-Dülmer, C., Wiedensohler, A., & Herrmann, H. (2011). Seasonal and diurnal variations of particulate nitrate and organic matter at the IfT research station Melpitz. *Atmospheric Chemistry and Physics*, *11*(24), 12,579–12,599. https://doi.org/10.5194/acp-11-12579-2011

Presto, A. A., Miracolo, M. A., Donahue, N. M., & Robinson, A. L. (2010). Secondary organic aerosol formation from high-NO_x photo-oxidation of low volatility precursors: *n*-alkanes. *Environmental Science & Technology*, *44*(6), 2029–2034. https://doi.org/10.1021/es903712r

Pye, H. O. T., & Seinfeld, J. H. (2010). A global perspective on aerosol from low-volatility organic compounds. *Atmospheric Chemistry and Physics*, *10*(9), 4377–4401. https://doi.org/10.5194/acp-10-4377-2010

Pye, H. O. T., Chan, A. W. H., Barkley, M. P., & Seinfeld, J. H. (2010). Global modeling of organic aerosol: The importance of reactive nitrogen (NO_x and NO_3). *Atmospheric Chemistry and Physics*, *10*(22), 11,261–11,276. https://doi.org/10.5194/acp-10-11261-2010

Ren, X., Brune, W. H., Mao, J., Mitchell, M. J., Lesher, R. L., Simpas, J. B., et al. (2006). Behavior of OH and HO_2 in the winter atmosphere in New York City. *Atmospheric Environment*, *40*, 252–S263. https://doi.org/10.1016/j.atmosenv.2005.11.073

Rengarajan, R., Sarin, M. M., & Sudheer, A. K. (2007). Carbonaceous and inorganic species in atmospheric aerosols during wintertime over urban and high-altitude sites in North India. *Journal of Geophysical Research*, *112*, D21307. https://doi.org/10.1029/2006JD008150

Rengarajan, R., Sudheer, A. K., & Sarin, M. M. (2011). Aerosol acidity and secondary organic aerosol formation during wintertime over urban environment in western India. *Atmospheric Environment*, *45*(11), 1940–1945. https://doi.org/10.1016/j.atmosenv.2011.01.026

Rienecker, M. M., Suarez, M. J., Todling, R., Bacmeister, J., Takacs, L., Liu, H.-C., et al. (2008). The GEOS-5 data assimilation system-documentation of versions 5.0.1, 5.1.0, and 5.2.0, NASA Tech Rep TM-2008-104606 27 (December). Retrieved from https://gmao.gsfc.nasa.gov/pubs/docs/Rienecker369.pdf

Robinson, A. L., Donahue, N. M., Shrivastava, M. K., Weitkamp, E. A., Sage, A. M., Grieshop, A. P., et al. (2007). Rethinking organic aerosols: Semivolatile emissions and photochemical aging. *Science*, *315*(5816), 1259–1262. https://doi.org/10.1126/science.1133061

Saide, P. E., Peterson, D. A., da Silva, A., Anderson, B., Ziemba, L. D., Diskin, G., et al. (2015). Revealing important nocturnal and day-to-day variations in fire smoke emissions through a multiplatform inversion. *Geophysical Research Letters*, *42*, 3609–3618. https://doi.org/10.1002/2015GL063737

Salcedo, D., Onasch, T. B., Dzepina, K., Canagaratna, M. R., Zhang, Q., Huffman, J. A., et al. (2006). Characterization of ambient aerosols in Mexico City during the MCMA-2003 campaign with Aerosol Mass Spectrometry: Results from the CENICA supersite. *Atmospheric Chemistry and Physics*, *6*(4), 925–946. https://doi.org/10.5194/acp-6-925-2006

Seibert, P., & Frank, A. (2004). Source-receptor matrix calculation with a Lagrangian particle dispersion model in backward mode. *Atmospheric Chemistry and Physics*, *4*(1), 51–63. https://doi.org/10.5194/acp-4-51-2004

Shrivastava, M., Cappa, C. D., Fan, J., Goldstein, A. H., Guenther, A. B., Jimenez, J. L., et al. (2017). Recent advances in understanding secondary organic aerosol: Implications for global climate forcing. *Reviews of Geophysics*, *55*, 509–559. https://doi.org/10.1002/2016RG000540

Song, X. H., Polissar, A. V., & Hopke, P. K. (2001). Sources of fine particle composition in the northeastern US. *Atmospheric Environment*, *35*(31), 5277–5286. https://doi.org/10.1016/S1352-2310(01)00338-7

Sorooshian, A., Brechtel, F., Ma, Y., Weber, R., Corless, A., Flagan, R., & Seinfeld, J. (2006). Modeling and characterization of a particle-into-liquid sampler (PILS). *Aerosol Science and Technology*, *40*(6), 396–409. https://doi.org/10.1080/02786820600632282

Stohl, A., & Thomson, D. J. (1999). A density correction for Lagrangian particle dispersion models. *Boundary-Layer Meteorology*, *90*(1), 155–167. https://doi.org/10.1023/A:1001741110696

Stohl, A., Hittenberger, M., & Wotawa, G. (1998). Validation of the lagrangian particle dispersion model FLEXPART against large-scale tracer experiment data. *Atmospheric Environment*, *32*(24), 4245–4264. https://doi.org/10.1016/S1352-2310(98)00184-8

Stohl, A., Forster, C., Frank, A., Seibert, P., & Wotawa, G. (2005). Technical note: The Lagrangian particle dispersion model FLEXPART version 6.2. *Atmospheric Chemistry and Physics*, *5*(9), 2461–2474. https://doi.org/10.5194/acp-5-2461-2005

Strader, R., Lurmann, F., & Pandis, S. N. (1999). Evaluation of secondary organic aerosol formation in winter. *Atmospheric Environment*, *33*(29), 4849–4863. https://doi.org/10.1016/S1352-2310(99)00310-6

Strapp, J. W., Leaitch, W. R., & Liu, P. S. K. (1992). Hydrated and dried aerosol-size-distribution measurements from the particle measuring systems FSSP-300 probe and the deiced PCASP-100X probe. *Journal of Atmospheric and Oceanic Technology*, *9*(5), 548–555. https://doi.org/10.1175/1520-0426(1992)009<0548:HADASD>2.0.CO;2

Sullivan, A. P., Frank, N., Kenski, D. M., & Collett, J. L. (2011). Application of high-performance anion-exchange chromatography-pulsed amperometric detection for measuring carbohydrates in routine daily filter samples collected by a national network: 2. Examination of

sugar alcohols/polyols, sugars, and anhydrosugars in the upper Midwest. *Journal of Geophysical Research*, *116*, D08303. https://doi.org/10.1029/2010JD014169

Sullivan, A. P., Frank, N., Onstad, G., Simpson, C. D., & Collett, J. L. (2011). Application of high-performance anion-exchange chromatography–pulsed amperometric detection for measuring carbohydrates in routine daily filter samples collected by a national network: 1. Determination of the impact of biomass burning in the upper Midwest. *Journal of Geophysical Research*, *116*, D08302. https://doi.org/10.1029/2010JD014166

Sullivan, A. P., May, A. A., Lee, T., McMeeking, G. R., Kreidenweis, S. M., Akagi, S. K., et al. (2014). Airborne characterization of smoke marker ratios from prescribed burning. *Atmospheric Chemistry and Physics*, *14*(19), 10,535–10,545. https://doi.org/10.5194/acp-14-10535-2014

Sullivan, A. P., Guo, H., Schroder, J. C., Campuzano-Jost, P., Jimenez, J. L., Campos, T., et al. (2017). Comparison of airborne-based measurements of biomass burning markers levoglucosan and aerosol mass spectrometer m/z 60 and the role of residential burning during the WINTER campaign. The American Association for Aerosol Research Annual Conference Abstracts (talk: 5CA.5). Retrieved from http://aaarabstracts.com/2017/viewabstract.php?pid=236

Sun, Y.-L., Zhang, Q., Schwab, J. J., Demerjian, K. L., Chen, W. N., Bae, M. S., et al. (2011). Characterization of the sources and processes of organic and inorganic aerosols in New York city with a high-resolution time-of-flight aerosol mass apectrometer. *Atmospheric Chemistry and Physics*, *11*(4), 1581–1602. https://doi.org/10.5194/acp-11-1581-2011

Takegawa, N., Miyazaki, Y., Kondo, Y., Komazaki, Y., Miyakawa, T., Jimenez, J. L., et al. (2005). Characterization of an Aerodyne Aerosol Mass Spectrometer (AMS): Intercomparison with other aerosol instruments. *Aerosol Science and Technology*, *39*(8), 760–770. https://doi.org/10.1080/02786820500243404

Takegawa, N., Miyakawa, T., Kondo, Y., Blake, D. R., Kanaya, Y., Koike, M., et al. (2006). Evolution of submicron organic aerosol in polluted air exported from Tokyo. *Geophysical Research Letters*, *33*, L15814. https://doi.org/10.1029/2006GL025815

Tan, P. V., Evans, G. J., Tsai, J., Owega, S., Fila, M. S., Malpica, O., & Brook, J. R. (2002). On-line analysis of urban particulate matter focusing on elevated wintertime aerosol concentrations. *Environmental Science & Technology*, *36*(16), 3512–3518. https://doi.org/10.1021/es011448i

Toon, O. B., Maring, H., Dibb, J., Ferrare, R., Jacob, D. J., Jensen, E. J., et al. (2016). Planning, implementation, and scientific goals of the Studies of Emissions and Atmospheric Composition, Clouds and Climate Coupling by Regional Surveys (SEAC^{4}RS) field mission. *Journal of Geophysical Research: Atmospheres*, *121*, 4967–5009. https://doi.org/10.1002/2015JD024297

Tsigaridis, K., Daskalakis, N., Kanakidou, M., Adams, P. J., Artaxo, P., Bahadur, R., et al. (2014). The AeroCom evaluation and intercomparison of organic aerosol in global models. *Atmospheric Chemistry and Physics*, *14*(19), 10,845–10,895. https://doi.org/10.5194/acp-14-10845-2014

Tsimpidi, A. P., Karydis, V. A., Pandis, S. N., & Lelieveld, J. (2016). Global combustion sources of organic aerosols: Model comparison with 84 AMS factor-analysis data sets. *Atmospheric Chemistry and Physics*, *16*(14), 8939–8962. https://doi.org/10.5194/acp-16-8939-2016

Ulbrich, I. M., Canagaratna, M. R., Zhang, Q., Worsnop, D. R., & Jimenez, J. L. (2009). Interpretation of organic components from positive matrix factorization of aerosol mass spectrometric data. *Atmospheric Chemistry and Physics*, *9*(9), 2891–2918. https://doi.org/10.5194/acp-9-2891-2009

Van Krevelen, D. W. (1950). Graphical-statistical method for the study of structure and reaction processes of coal. *Fuel*, *24*, 269–284.

Viana, M., Chi, X., Maenhaut, W., Querol, X., Alastuey, A., Mikuška, P., & Večeřa, Z. (2006). Organic and elemental carbon concentrations in carbonaceous aerosols during summer and winter sampling campaigns in Barcelona, Spain. *Atmospheric Environment*, *40*(12), 2180–2193. https://doi.org/10.1016/j.atmosenv.2005.12.001

Volkamer, R., Jimenez, J. L., San Martini, F., Dzepina, K., Zhang, Q., Salcedo, D., et al. (2006). Secondary organic aerosol formation from anthropogenic air pollution: Rapid and higher than expected. *Geophysical Research Letters*, *33*, L17811. https://doi.org/10.1029/2006GL026899

Wagner, N. L., Dube, W. P., Washenfelder, R. A., Young, C. J., Pollack, I. B., Ryerson, T. B., & Brown, S. S. (2011). Diode laser-based cavity ring-down instrument for NO_3, N_2O_5, NO, NO_2 and O_3 from aircraft. *Atmospheric Measurement Techniques*, *4*(6), 1227–1240. https://doi.org/10.5194/amt-4-1227-2011

Wagner, N. L., Brock, C. A., Angevine, W. M., Beyersdorf, A., Campuzano-Jost, P., Day, D., et al. (2015). In situ vertical profiles of aerosol extinction, mass, and composition over the southeast United States during SENEX and SEAC^{4}RS: Observations of a modest aerosol enhancement aloft. *Atmospheric Chemistry and Physics*, *15*(12), 7085–7102. https://doi.org/10.5194/acp-15-7085-2015

Warneke, C., de Gouw, J. A., Goldan, P. D., Kuster, W. C., Williams, E. J., Lerner, B. M., et al. (2004). Comparison of daytime and nighttime oxidation of biogenic and anthropogenic VOCs along the New England coast in summer during New England Air Quality Study 2002. *Journal of Geophysical Research*, *109*, D10309. https://doi.org/10.1029/2003JD004424

Warneke, C., McKeen, S. A., de Gouw, J. A., Goldan, P. D., Kuster, W. C., Holloway, J. S., et al. (2007). Determination of urban volatile organic compound emission ratios and comparison with an emissions database. *Journal of Geophysical Research*, *112*, D10S47. https://doi.org/10.1029/2006JD007930

Warneke, C., De Gouw, J. A., Holloway, J. S., Peischl, J., Ryerson, T. B., Atlas, E., et al. (2012). Multiyear trends in volatile organic compounds in Los Angeles, California: Five decades of decreasing emissions. *Journal of Geophysical Research*, *117*, D00V17. https://doi.org/10.1029/2012JD017899

Weber, R. J., Sullivan, A. P., Peltier, R. E., Russell, A., Yan, B., Zheng, M., et al. (2007). A study of secondary organic aerosol formation in the anthropogenic-influenced southeastern United States. *Journal of Geophysical Research*, *112*, D13302. https://doi.org/10.1029/2007JD008408

Weimer, S., Drewnick, F., Hogrefe, O., Schwab, J. J., Rhoads, K., Orsini, D., et al. (2006). Size-selective nonrefractory ambient aerosol measurements during the Particulate Matter Technology Assessment and Characterization Study—New York 2004 Winter Intensive in New York City. *Journal of Geophysical Research*, *111*, D18305. https://doi.org/10.1029/2006JD007215

Wild, R. J., Edwards, P. M., Dubé, W. P., Baumann, K., Edgerton, E. S., Quinn, P. K., et al. (2014). A measurement of total reactive nitrogen, NO_y, together with NO_2, NO, and O_3 via cavity ring-down spectroscopy. *Environmental Science & Technology*, *48*(16), 9609–9615. https://doi.org/10.1021/es501896w

WINTER-Data (2018). WINTER data repository. Retrieved from https://data.eol.ucar.edu/dataset/explore?projects=483, (Accessed 2 February 2018).

WINTER (2018). WINTER information. Retrieved from https://www.eol.ucar.edu/field_projects/winter, (Accessed 2 February 2018).

Womack, C. C., Neuman, J. A., Veres, P. R., Eilerman, S. J., Brock, C. A., Decker, Z. C. J., et al. (2017). Evaluation of the accuracy of thermal dissociation CRDS and LIF techniques for atmospheric measurement of reactive nitrogen species. *Atmospheric Measurement Techniques*, *10*(5), 1911–1926. https://doi.org/10.5194/amt-10-1911-2017

Xu, J., Shi, J., Zhang, Q., Ge, X., Canonaco, F., Prévôt, A. S. H., et al. (2016). Wintertime organic and inorganic aerosols in Lanzhou, China: Sources, processes, and comparison with the results during summer. *Atmospheric Chemistry and Physics*, *16*(23), 14,937–14,957. https://doi.org/10.5194/acp-16-14937-2016

Xu, L., Suresh, S., Guo, H., Weber, R. J., & Ng, N. L. (2015). Aerosol characterization over the southeastern United States using high-resolution aerosol mass spectrometry: Spatial and seasonal variation of aerosol composition and sources with a focus on organic nitrates. *Atmospheric Chemistry and Physics*, *15*(13), 7307–7336. https://doi.org/10.5194/acp-15-7307-2015

Yang, Q., Easter, R. C., Campuzano-Jost, P., Jimenez, J. L., Fast, J. D., Ghan, S. J., et al. (2015). Aerosol transport and wet scavenging in deep convective clouds: A case study and model evaluation using a multiple passive tracer analysis approach. *Journal of Geophysical Research: Atmospheres*, *120*, 8448–8468. https://doi.org/10.1002/2015JD023647

Zhang, Q., Jimenez, J. L., Canagaratna, M. R., Allan, J. D., Coe, H., Ulbrich, I., et al. (2007). Ubiquity and dominance of oxygenated species in organic aerosols in anthropogenically-influenced Northern Hemisphere midlatitudes. *Geophysical Research Letters*, *34*, L13801. https://doi.org/10.1029/2007GL029979

Zhang, Q., Jimenez, J. L., Canagaratna, M. R., Ulbrich, I. M., Ng, N. L., Worsnop, D. R., & Sun, Y. (2011). Understanding atmospheric organic aerosols via factor analysis of aerosol mass spectrometry: A review. *Analytical and Bioanalytical Chemistry*, *401*(10), 3045–3067. https://doi.org/10.1007/s00216-011-5355-y

Zhang, X., Hecobian, A., Zheng, M., Frank, N. H., & Weber, R. J. (2010). Biomass burning impact on $PM_{2.5}$ over the southeastern US during 2007: integrating chemically speciated FRM filter measurements, MODIS fire counts and PMF analysis. *Atmospheric Chemistry and Physics*, *10*(14), 6839–6853. https://doi.org/10.5194/acp-10-6839-2010

Zhang, Y., Tang, L., Yu, H., Wang, Z., Sun, Y., Qin, W., et al. (2015). Chemical composition, sources and evolution processes of aerosol at an urban site in Yangtze River Delta, China during wintertime. *Atmospheric Environment*, *123*, 339–349. https://doi.org/10.1016/j.atmosenv.2015.08.017

Zhao, Y., Hennigan, C. J., May, A. A., Tkacik, D. S., de Gouw, J. A., Gilman, J. B., et al. (2014). Intermediate-volatility organic compounds: A large source of secondary organic aerosol. *Environmental Science & Technology*, *48*(23), 13,743–13,750. https://doi.org/10.1021/es5035188

Zhou, S., Collier, S., Xu, J., Mei, F., Wang, J., Lee, Y.-N., et al. (2016). Influences of upwind emission sources and atmospheric processing on aerosol chemistry and properties at a rural location in the Northeastern U.S. *Journal of Geophysical Research: Atmospheres*, *121*, 6049–6065. https://doi.org/10.1002/2015JD024568